ANALYZING EL NIÑO- SOUTHERN OSCILLATION SENSITIVITY IN A LARGE ENSEMBLE OF OCEAN REANALYSES

A Thesis

by

KELLEY BRADLEY

Submitted to the Office of Graduate and Professional Studies of
Texas A&M University
in partial fulfillment of the requirements for the degree of

MASTER OF SCIENCE

Chair of Committee,	Benjamin Giese
Committee Members,	Achim Stössel
	Ping Chang
	Howard Seidel
Head of Department,	Debbie Thomas

May 2015

Major Subject: Oceanography

ABSTRACT

A 56-member ensemble of ocean reanalyses is used to explore strong El Niño events in two 5-year periods, 1916 to 1920 and 1996 to 2000, that have markedly different quantities of observations. To generate the 56 forcing fields, we use a 56 member atmospheric reanalysis (20CRv2 system). Prescribed as boundary conditions were 8 different sea surface temperature (SST) estimates from an ocean reanalysis system, SODA with sparse input (SODA.si1), resulting in 8 sets of 7 ensemble members each. The 56 atmospheric reanalyses were used to force an ocean reanalysis for the same two time periods.

The ocean reanalyses, SODA_XP, are used to explore ENSO sensitivity in the tropical Pacific Ocean. Results from the two periods show two sources of uncertainty in the reanalyses. One source is the inherent atmospheric noise that partially causes the representation of the same ENSO event to vary widely in strength, duration, and location among the 56 ensemble members. For example, warming during the 1918/1919 event in some members is far in the eastern equatorial Pacific Ocean while in other members the major warming is in the central Pacific. The other source of uncertainty comes from prescribing SST to the atmosphere, and is primarily responsible for differences seen among ensemble members. During the well-observed 1996-2000 period, the ensemble variance is considerably smaller than that of the 1916-1920 period, thus a markedly reduced level of uncertainty. Similarities among the results of each atmospheric reanalysis set generated with the same SODAsi.1 SST suggest that the state estimates are

strongly dependent upon the SST boundary condition. The results add to what is previously known about ENSO in order to improve ENSO predictability, as well as highlight the importance of loosely coupling ocean and atmosphere reanalyses to adequately represent the range of possible climate states in periods of few observations.

ACKNOWLEDGEMENTS

I would like to thank my committee chair, Dr. Giese, my committee members, Dr. Stössel, Dr. Chang, and Dr. Seidel, and Dr. Compo for their guidance, support, and patience throughout the course of this research.

Thanks also go to my friends and the department faculty and staff for making my time at Texas A&M University a great experience. I also want to extend my gratitude to the National Science Foundation, which provided the funding to support me during my graduate career.

Finally, thanks to Mom, Dad, Grandma, Mike, and Chris for their constant love and encouragement throughout my academic journey.

NOMENCLATURE

ENSO	El Niño/Southern Oscillation
SST	Sea Surface Temperature
SODAsi.1	8 ensemble member ocean reanalyses conducted for 1871-2008.
SODA_XP	56 ensemble member ocean reanalyses conducted for 1916-1920 and 1996-2000.
20CRv2	Twentieth Century Reanalysis Version 2
20CRv2 Scout 3.3.1	Twentieth Century Reanalysis Version 2 subset forced with 8 members of SODAsi.1.
HadISST1.1	Hadley Centre Sea Ice and Sea Surface Temperature reconstructed dataset.
SODA	Simple Ocean Data Assimilation
POP	Parallel Ocean Program
ICOADS2.5	International Comprehensive Ocean-Atmosphere dataset version 2.5
Group #	Set of ensemble members forced with the same SODAsi.1 SST
WWB	Westerly Wind Bursts
DJF	Average over December, January, and February
Niño3.4	Region from 5°N to 5°S and 120°W to 170°W over which anomalies are constructed

TABLE OF CONTENTS

LIST OF FIGURES

Page

1. INTRODUCTION

Global climate change, an important scientific issue, is an underlying focus of many international research endeavors. It is now widely accepted that the average global surface temperature is increasing. What is not understood as well is how the Earth's climate system will respond to global warming forcing on both short and long-term timescales. Using numerical and statistical models to establish potential responses aids in understanding how climate change arises, helps to improve climate predictions, and influences policy decisions worldwide. Some of these models are coupled between the ocean and atmosphere to more comprehensively resolve potential climates. However, many of these coupled models are hampered by bias and model drift, resulting in climate states that are not realistic.

Of particular interest is the response of the tropical Pacific Ocean because of its significance to global climate. The most prominent phenomenon in the tropical Pacific Ocean affecting climate worldwide is the El Niño/Southern Oscillation (ENSO). The equatorial Pacific has cooler water in the eastern Pacific and warmer water in the western Pacific, thus inducing a basin-wide zonal sea surface temperature (SST) gradient. Accompanying this SST gradient is a pressure gradient across the equatorial Pacific that has a tendency to fluctuate, which affects regional weather patterns. In his 1924 paper discussing world weather correlations, Sir Gilbert Walker named these observed pressure variations between stations in the eastern Pacific Ocean and the Indian Ocean the "Southern Oscillation" [*Walker*, 1924]. The aforementioned east-west thermal

gradient is coupled to the Southern Oscillation resulting in a thermally direct circulation in the equatorial plane. Jacob Bjerknes first discovered the cross-basin circulation appropriately naming it the Walker Circulation in 1969 [*Bjerknes*, 1969]. The Walker Circulation is characterized by westward low-level flow as an extension of the equatorial trade winds, rising motion, and deep convection in the extreme western Pacific regions; eastward return flow *drifts* in the upper atmosphere with sinking motion of this return flow in the far eastern Pacific.

This circulation typically brings heavy precipitation to the west side of the basin and high-pressure subsidence to the east side of the basin. However, deviations from typical sea surface temperatures can have large-scale impacts on regional ocean processes, as well as on global weather patterns and overall climate. Bjerknes first determined the connection between SST anomalies and changes in precipitation with large-scale variations of the equatorial trade winds; these variations ultimately reflect the major oscillations of the Southern Oscillation pressure system. As a result, warm SST anomalies, originally known as El Niño, became the El Niño Southern Oscillation, or ENSO [*Rasmusson and Wallace*, 1983]. An El Niño event is characterized by warm SST anomalies of 0.5°C or above observed for three consecutive months in the Niño3.4 region, which is defined as a spatial box from 120°W - 170°W and 5°N - 5°S. The warm SST anomalies result in a weaker east-west thermal gradient that causes the westward surface flow to weaken and wind anomalies to appear. This disruption of the Walker Circulation moves the area of heavy precipitation eastward along the equator causing drought in regions where there usually is ample rain and causing flooding in regions

where the climate is usually arid. The western Pacific warm pool of SST expands eastward to cover a large portion of the tropics, and upwelling that occurs off the coast of South America weakens resulting in warm temperature anomalies that define an El Niño event. Due to the teleconnections between the equatorial Pacific, extratropical, and mid-latitude regions, these areas also experience significant climate anomalies during an El Niño event. Impacts of a La Niña event, the cold phase of ENSO, are typically the opposite of El Niño as the easterly trade winds strengthen, enhancing upwelling, and pushing the warm pool further west along the equator.

Although the impacts of ENSO are well documented [*Schubert et al*.,2004; *Seager et al*., 2005; *Vecchi and Soden*, 2007a; *Chavez et al*., 2011], there is still much uncertainty in forecasting ENSO and how ENSO will respond to climate change. Investigating these questions requires long-term SST records that are not available in observational data sets alone. *Ray and Giese* [2012] demonstrate that even 34 El Niño events are not enough to determine trends in ENSO frequency; thus time series that contain hundreds of El Niño events are required. To address the need for long-term SST records, several reconstructed SST data sets have been developed. These reconstructions include HadISST1.1 [*Rayner et al.*, 2003], ERSST [*Smith et al.,* 2008], and Kaplan SST [*Kaplan et al.,* 1998] that cover from 1850 to the present. Reconstructed data sets are created using empirical orthogonal functions [*Rayner et al.*, 2003] on data from the last half of the twentieth century to extrapolate SST data for periods of sparse observations. However, *Giese and Ray* [2011] found that these statistical methods used to generate

reconstructed SST datasets underestimate ENSO spatial patterns, thus limiting their value for long-term variability studies.

An alternative approach is run reanalyses, which combines observations and a model through the process of data assimilation. Algorithms for this have been developed to merge sparse observational data sets with models to provide an estimation of the time evolving state of the atmosphere and the oceans. The Twentieth Century Reanalysis (20CRv2) [*Compo et al*., 2011], an ensemble-based atmospheric reanalysis dataset, is one of these data assimilation schemes used to hindcast as far back as 1871. The first run of 20CRv2 used a single estimate of SST from HadISST1.1 for the oceanic boundary conditions resulting in limited ocean variability. To enhance the variability of oceanic feedback to the atmosphere reanalysis, ensembles of the Simple Ocean Data Assimilation (SODA) are used as forcing instead of HadISST1.1. There are several versions of SODA spanning the 20th Century [*Giese et al*., 2010; *Giese and Ray*, 2011; *Ray and Giese*, 2012, *Yang and Giese,* 2013]. Analysis of a recent version, SODAsi.1 (where si stands for sparse input), shows considerable ENSO variability from different atmospheric ensemble members. This raises the question of how the atmosphere reanalysis may respond to different SST estimates. In this research, we explore the sensitivity of ocean reanalysis to atmosphere forcing generated with SST estimates that encompass a greater range of uncertainty to better capture SST estimates found in nature.

2. METHODS

To test the described hypotheses we conduct several new reanalyses. The reanalyses use the SODA methodology [*Carton and Giese*, 2008] consisting of the Parallel Ocean Program (POP) [*Smith et al*., 1992] ocean model and SODA algorithm. Details of the SODA system are described elsewhere [*Carton and Giese*, 2008]. Briefly, the POP ocean model is used with horizontal resolution that is 0.4° (zonal) × 0.25° (meridional) with 40 vertical levels and 10-m spacing near the surface. In order to resolve the Arctic Ocean, the model covers the global domain with a distorted grid in the Northern Hemisphere. The meridional resolution increases poleward to reduce the grid anisotropy that results from the Mercator coordinate grid due to the convergence of meridians at high latitudes. Horizontal mixing is addressed using biharmonic parameterization, whereas K-profile parameterization is used for vertical mixing. River input is included with climatological seasonal discharge, and there is no explicit sea ice model; however, the surface heat flux is modified when the surface temperature reaches the freezing point of seawater.

Carton and Giese [2008] describe the data assimilation process for observations using a sequential 10-day update cycle. A simulation is run for 5 days from day t to day t+5 producing a first guess. At day t+5, an analysis combining the first guess and the observations yields an estimate of temperature and salinity. The differences between the analysis and the first guess are calculated and referred to as innovations. The model is then restarted at day t and integrated to day t+10 adding the calculated temperature and

salinity innovations at every time step. The run proceeds by repeating this procedure at t+10 for the length of the assimilation. Model output consists of five-day averages mapped on to a uniform global 0.5°x0.5° horizontal grid using the horizontal grid spherical coordinate remapping and interpolation package [*Jones* 1999].

For this project, a 56 member ensemble of ocean reanalyses using the SODA methodology is conducted (SODA_XP). SODA_XP is run for two 5-year periods of particular interest (1916-1920 and 1996-2000). These periods were chosen not only because they both contain a strong ENSO event, but also the earlier period had very few observations, while the latter period is well observed. There are several previous versions of SODA spanning the 20th Century [*Giese et al*., 2010; *Giese and Ray*, 2011; *Ray and Giese*, 2012]; however, these earlier versions of SODA rely on forcing from an ensemble mean of an ensemble-based atmospheric reanalysis dataset [*Compo et al*., 2011]. This approach is acceptable in times for which there are numerous observations as discussed by *Yang and Giese* [2013]. Conversely, using the ensemble mean results in large biases due to weather noise being dampened in times of sparse observations but is retained in times of abundant observations.

SODA_XP is unique compared to previous versions of SODA with one of the most important differences being how the atmospheric forcing fields were generated from 20CRv2. The model used by 20CRv2, as described by *Compo et al.* [2011], is a coupled atmosphere-land model based on the National Center for Environmental Prediction (NCEP) Global Forecast System (GFS). The model has horizontal and vertical resolutions of 62 total spectral wave numbers and 28 hybrid sigma-pressure

levels respectively. As previously mentioned, the HadISST1.1 dataset [*Rayner et al.,* 2003] provides the surface boundary conditions of SST and sea ice concentrations for 20CRv2 by interpolating monthly to daily averages. Assimilated surface- and sea-level pressure observations are from the International Surface Pressure Databank (ISPD) version 2. These data come from land stations, marine observations, and tropical cyclone 'best track' pressure observations and reports. The International Comprehensive Ocean-Atmosphere Data Set version 2.5 (ICOADS 2.5) [*Woodruff et al.,* 2011] provides sea level pressure (SLP) from marine observations for 1846-1951, and ICOADS 2.4 provides SLP for 1952-2008. The International Best Track Archive for Climate Stewardship (IBTrACs) implements the tropical cyclone data. *Compo et al.* [2011] describe the quality control procedures conducted on ISPD observations prior to assimilation in 20CRv2.

The process of assimilation used by 20CRv2 is an Ensemble Kalman Filter algorithm based on an ensemble square root filter [*Whitaker and Hamill*, 2002; *Whitaker et al.,* 2004, *Compo et al.,* 2006; *Compo et al.,* 2011]. An ensemble of 56 nine-hour forecasts is generated, and 56 six-hour analyses are produced. Given that 20CRv2 is the first data set producing a synoptic analysis dating back to a sparsely observed 1871, estimating the uncertainty of all analysis fields at each time step results in an evaluation of the data set. Comparisons to other data sources, including radiosonde data and National Weather Prediction forecasts, show that 20CRv2 accurately encapsulates much of the observed variability in both weather and climate [*Compo et al*., 2011; *Brönnimann et al.,* 2011; *Brönnimann et al.,* 2012; *Compo et al*., 2013].

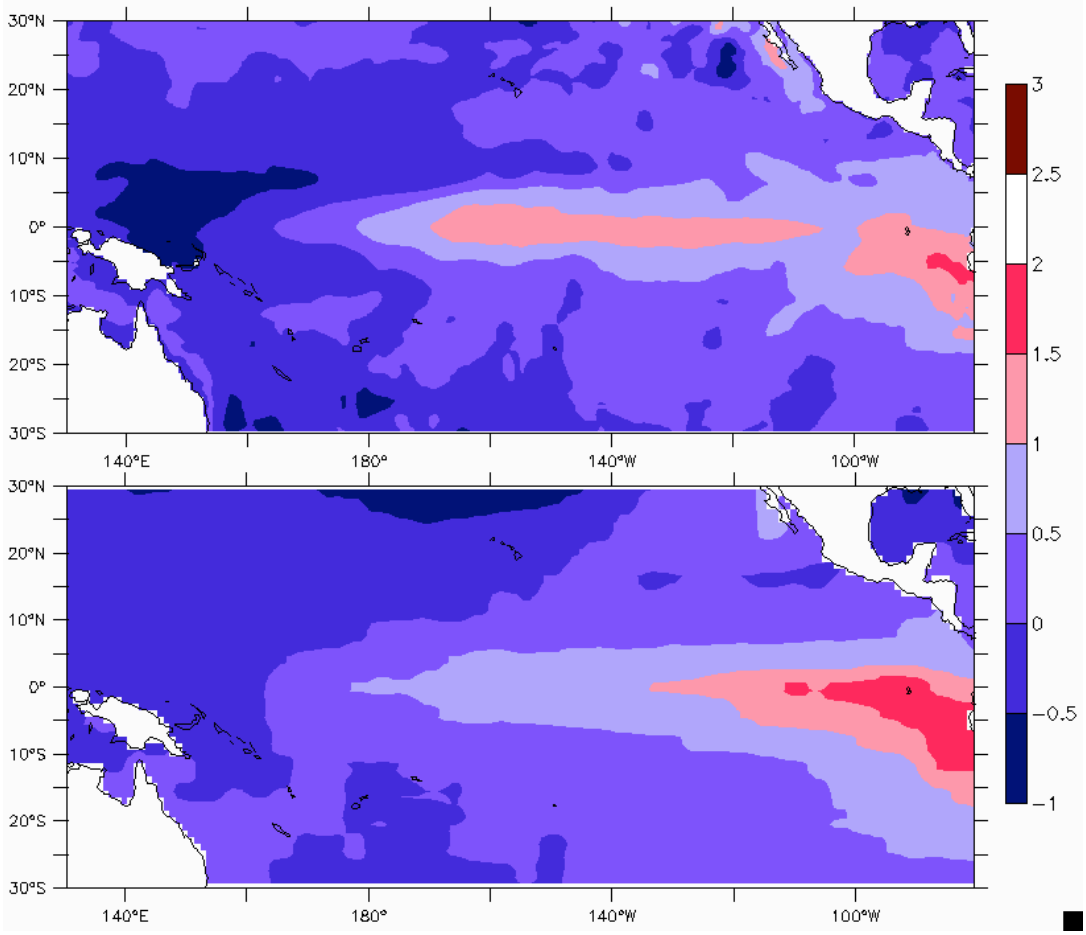

Figure 1. SST anomaly (°C) averaged for April 1918 through May 1919 from SODAsi.2 (top) and HadISST1.1 reconstruction dataset (bottom).

A significant drawback of 20CRv2 reanalysis is that all 56 ensemble members use the same HadISST1.1 estimate. Using a single SST field as forcing assumes that the SST field is equally well known through time. However, this assumption is incorrect because SST estimates for 150 years ago are not nearly as accurate as in recent estimates. Ideally, 20CRv2 would include a source of information about the error or

uncertainty in our knowledge of the SST field. As an example, the SST anomaly for April 1918 through May 1919 from a SODA assimilation (SODAsi.2) and HadISST1.1 reconstruction dataset is shown in Figure 1. It is evident that HadISST1.1 is considerably different than what is shown by the ocean reanalyses. In fact, the westward extent of the depicted El Niño is limited in the HadISST1.1 panel because at that time any SST observations were located along the South American coast [*Giese et al.,* 2010]. Increasing the number of ensemble members accounts for the changing uncertainty of SST estimates. SODA_XP's large ensemble of 56 members includes a source of error for SST.

The schematic in Figure 2 depicts iterative exchanges of forcing and subsequent historical reanalyses between SODA and 20CRv2 in an effort to loosely couple the ocean and atmosphere. In the original 20CRv2 reanalysis run, HadISST1.1, shown in Figure 1, was used as oceanic forcing for all 56 ensemble members. Out of the 56 20CRv2 members [*Whitaker et al*., 2004; *Compo et al*., 2006; *Compo et al*., 2011], 8 members were randomly selected as boundary conditions for a previous version of SODA, SODAsi.1, which produced 8 ensemble members of SODA assimilation. When using 20CRv2 variables for SODA boundary conditions, daily averages are computed from the atmospheric output. The surface wind stress is used to compute surface momentum fluxes, while solar radiation, specific humidity, cloud cover, 2m air temperature, precipitation, and 10m wind speed are used to calculate heat and freshwater fluxes. All of the ocean reanalysis ensemble members in SODAsi.1 and SODA_XP assimilate the same ocean observations via the same SODA assimilation system.

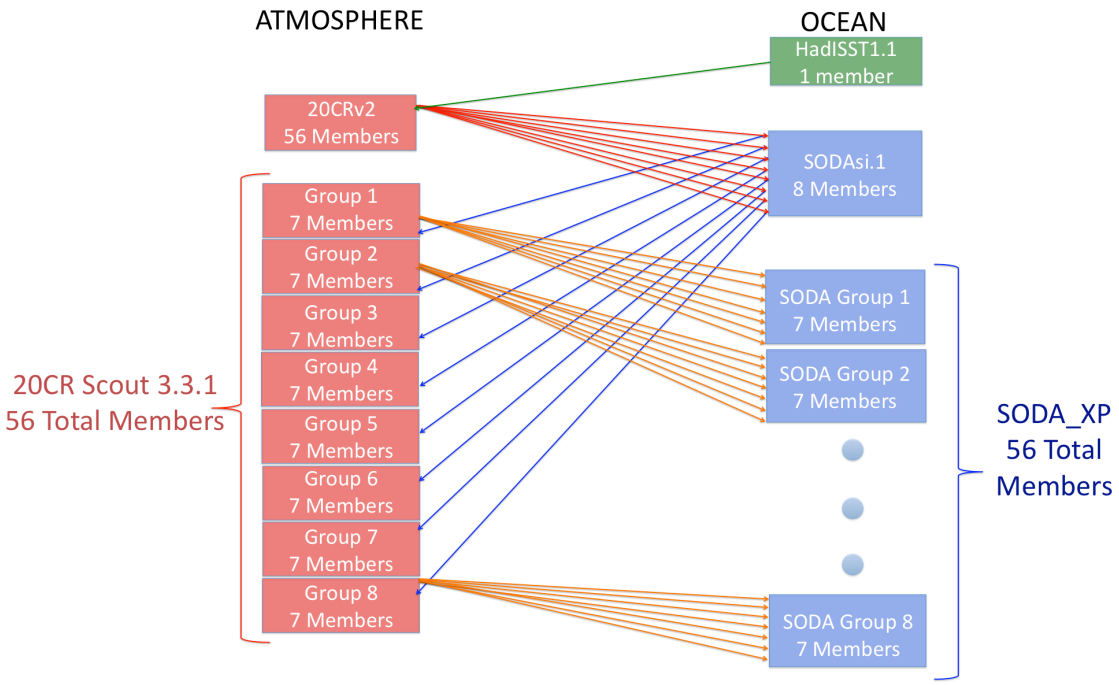

Figure 2. Schematic diagram showing the progression of reanalysis iterations between SODA and 20CRv2.

The 8 generated ensemble members of SODAsi.1 were used to force 20CRv2 again, but in a smaller subset spanning just two 5-year periods (1916-1920 and 1996-2000). These experiments are called 20CRv2 Scout 3.3.1. In order to generate the 56 ensemble members of 20CRv2 Scout 3.3.1, the 8 members from SODAsi.1 were used as forcing repeatedly in a sequential fashion (i.e. each SODAsi.1 ensemble member forced 7 different 20CRv2 Scout 3.3.1 ensemble members). This step is shown via the blue arrows in Figure 2.

These 56 members of 20CRv2 Scout 3.3.1 are used as forcing for SODA_XP. The 7 orange arrows coming from each red 20CRv2 Scout 3.3.1 box in Figure 2 represent the next step in the loosely coupled reanalyses. The resulting 56 ensembles of SODA_XP can then be divided into 8 different groups based on the same SST forcing previously used to force 20CRv2 Scout 3.3.1. For example, SODA_XP Group 1 refers to the 7 individual ensemble members that were all forced with SODAsi.1 SST ensemble member 1. The 8 rows of Table 1 illustrate how the ensembles are organized based on SODAsi.1 SST forcing. Each ensemble member of SODA_XP was labeled with 4 digits. The blue digits are the SODA_XP group number from 1 to 8, and the black digits refer to the ensemble member number within an individual group from 1 to 7. The red number in each box is the atmospheric ensemble number from 1 to 56.

SODAsi.1 SST							
ENS 1	01 01_01	09 01_02	17 01_03	25 01_04	33 01_05	41 01_06	49 01_07
ENS 2	02 02_01	10 02_02	18 02_03	26 02_04	34 02_05	42 02_06	50 02_07
ENS 3	03 03_01	11 03_02	19 03_03	27 03_04	35 03_05	43 03_06	51 03_07
ENS 4	04 04_01	12 04_02	20 04_03	28 04_04	36 04_05	44 04_06	52 04_07
ENS 5	05 05_01	13 05_02	21 05_03	29 05_04	37 05_05	45 05_06	53 05_07
ENS 6	06 06_01	14 06_02	22 06_03	30 06_04	38 06_05	46 06_06	54 06_07
ENS 7	07 07_01	15 07_02	23 07_03	31 07_04	39 07_05	47 07_06	55 07_07
ENS 8	08 08_01	16 08_02	24 08_03	32 08_04	40 08_05	48 08_06	56 08_07

Table 1. Labeling scheme for SODA_XP experiments

Additional differences among SODAsi.1, SODA_XP, and previous SODA runs include the observations assimilated into the reanalyses. SODAsi.1 and SODA_XP assimilate only SST from ICOADS 2.5, whereas older SODA versions use all available surface and subsurface observations for temperature and salinity. The available subsurface temperature and salinity profile data in SODA_XP is not assimilated in order to reduce spurious climate signals such as decadal climate variability resulting from the increasing number of hydrographic measurements since the 1950s. For this experiment, we applied the spatially and monthly time-varying bucket corrections used for HadISST1.1 [*Rayner et al*., 2003] to the ICOADS SST observations. As expected, there are fewer observations for 1916-1920 than for 1996-2000, but Figure 3 shows that the

few existing observations are mostly along the coast of South America and select shipping routes. In total, four sets of experiments were performed to complete SODA_XP. An assimilation and simulation were conducted for both time periods with each set having 56 ensemble members.

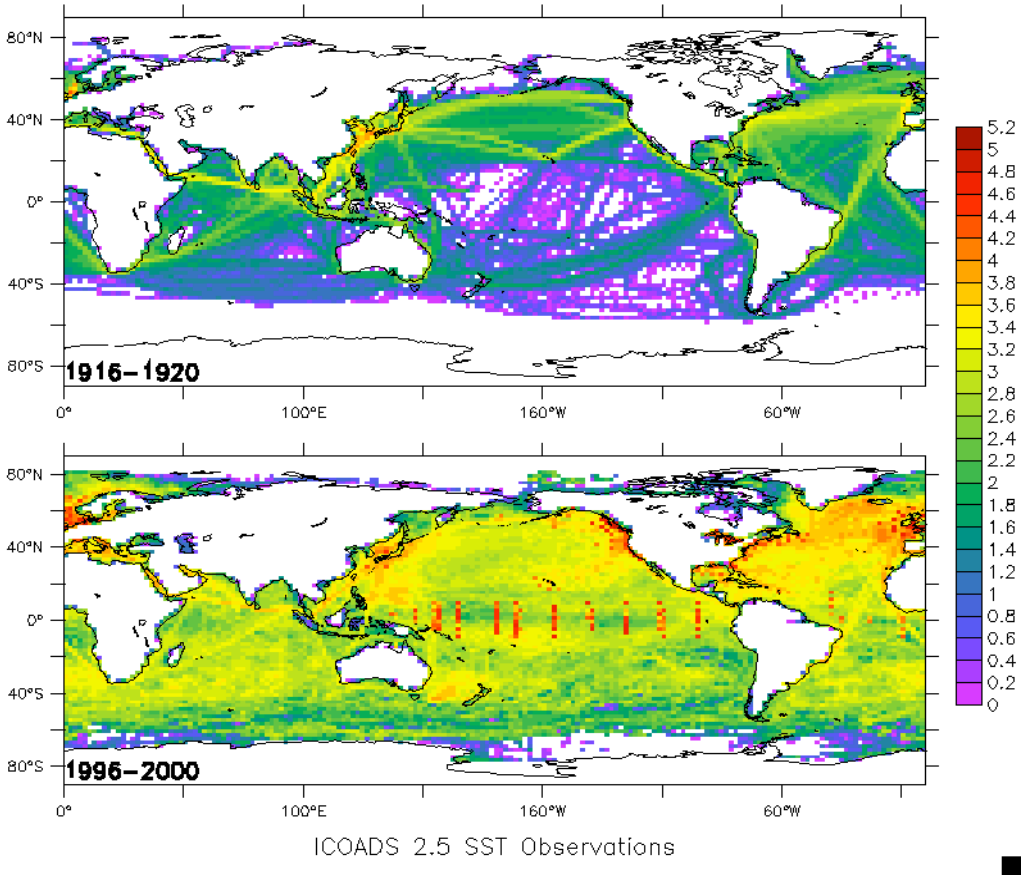

Figure 3. Log of the number of global SST observations for SODA_XP averaged over the two time periods.

3. RESULTS

3.1 1918/1919 El Niño

Analysis of the two 5-year periods is similar to a composite analysis, but instead of looking at different ENSO events, we analyze 56 different realizations of the same event. All ensemble members for the 1916-1920 period reveal an El Niño event in 1918/1919, but the strength, duration, and location of the event varies widely among members. The 56 member ensemble mean of zonal winds and SST anomaly are shown in Figure 4. The left hand panel depicts pulses of high frequency atmospheric variability, or westerly wind bursts (WWB), preceding the El Niño event as well as during the event. Wind anomalies are expected in individual members of a large ensemble set as it will capture the random variability, but since these wind anomalies persist in an ensemble mean of all 56 ensembles, it suggests they are of considerable importance to the formation, progression, and maturation of the El Niño event.

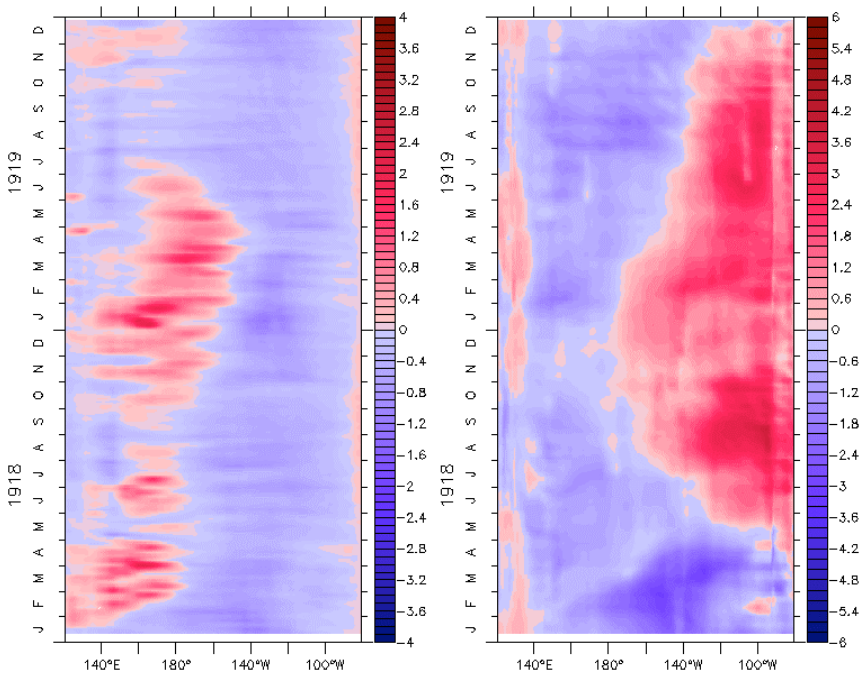

Figure 4. Zonal wind stress (N/m^2) (left panel) and SST (°C) (right panel) anomalies of the 56 ensemble mean for 1916 – 1920.

One of the main reasons for performing a large ensemble of reanalyses is to accurately capture the variability of the system(s) in question. Due to the immense resources involved in running extensive reanalyses for both the atmosphere and ocean, there is interest in how many ensemble members are actually necessary. Figures 4, 5 and 6 depict averages of ensemble members starting with 8 members and continuing to the full ensemble mean of 56 members. Among these four means for zonal wind stress and SST anomalies, there are not many differences. All of the panels in Figure 5 for zonal wind stress anomalies averaged over 8 ensemble members (left panel), 16 ensemble members (middle panel), and 32 ensemble members (right panel) illustrate high frequency bursts of wind. More specifically, the 8 ensemble member mean maintains

similar features in both zonal wind stress and SST anomaly fields compared with the full 56 ensemble member mean (Figure 4, left panel). This suggests that 8 ensemble members may be sufficient to capture the high frequency variability necessary to analyze ENSO.

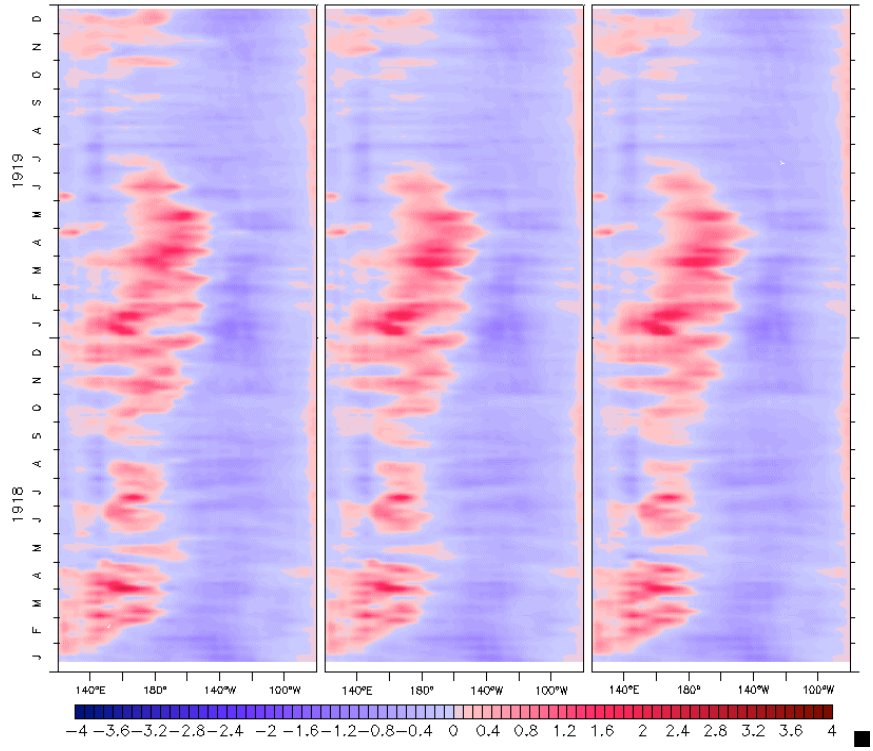

Figure 5. Zonal wind stress (N/m^2) anomalies of ensemble member means for 1916 – 1920. The left panel is an 8 member mean, middle panel is a 16 member mean, and the right panel is a 32 member mean.

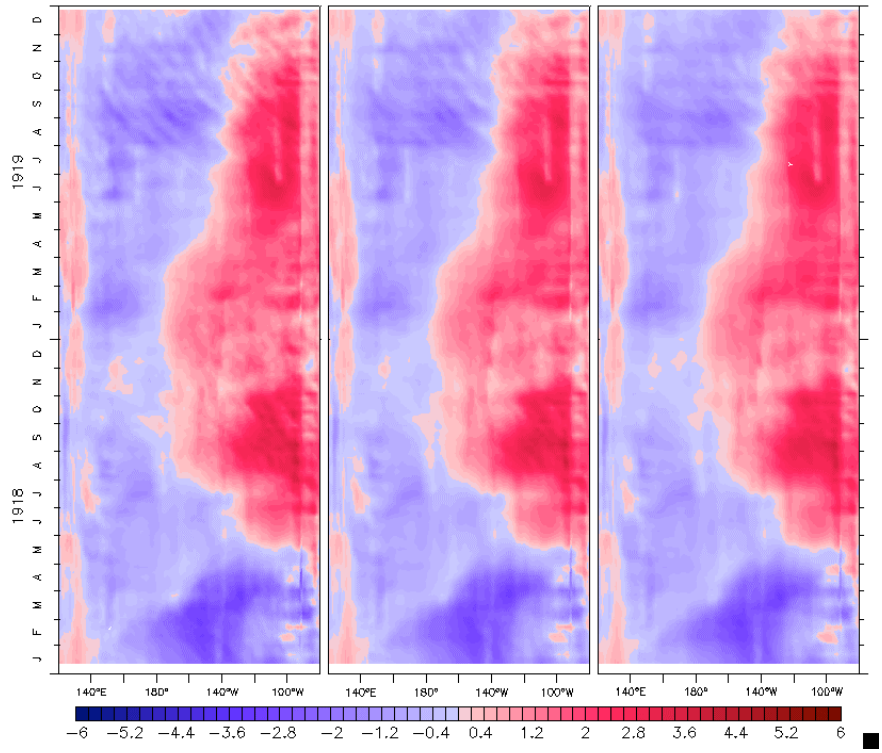

Figure 6. SST anomalies (°C) of ensemble member means for 1916 – 1920. The left panel is an 8 member mean, middle panel is a 16 member mean, and the right panel is a 32 member mean.

SODA_XP is a product of loosely coupled ocean and atmosphere reanalyses performed in an iterative fashion. It is hypothesized that the more iterations conducted, the more the solutions will converge to a "true state". Being that SODA_XP is the first loosely coupled product using the full atmospheric ensemble set of 20CRv2, there needs to be at least one, if not two, more ocean-atmosphere iterations to determine the presence of convergence. Comparisons could also be made to future versions of SODAsi in order to determine the level of convergence between the reanalyses.

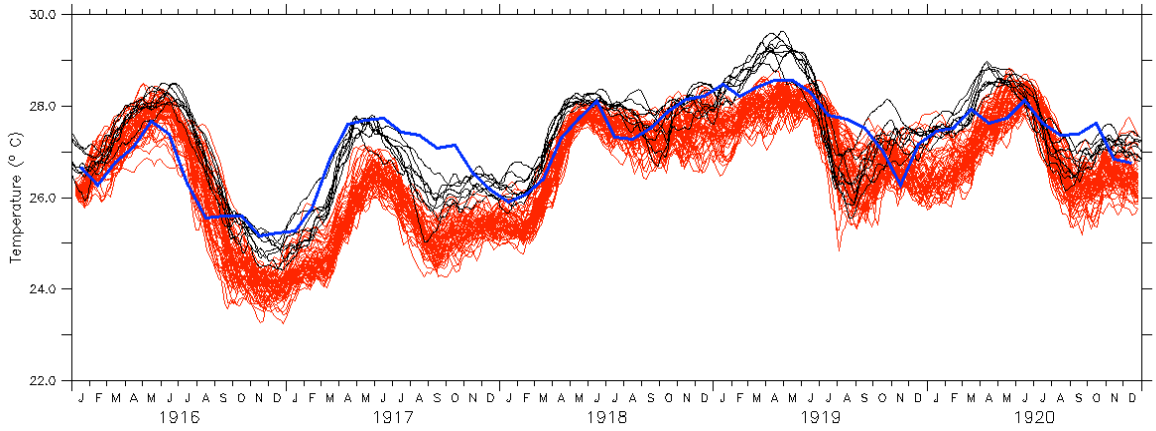

Figure 7. Niño3.4 SST (°C) for HadISST1.1 (blue), SODAsi.1 8 ensembles (black), and SODA_XP 56 ensembles (red) from 1916-1920.

The time series SST averaged over Niño3.4 for the iterations are shown in Figure 7. Figure 7 contains 56 red lines (one for each individual SODA_XP ensemble member), 8 black lines (one for each SODAsi.1 ensemble member), and 1 blue line for HadISST1.1. As expected, increasing the number of ensemble members illustrates the ensemble spread, which is not apparent in a single realization, such as HadISST1.1. SODA_XP is sometimes cooler than HadISST1.1, but interestingly sometimes warmer as well. This could be misinterpreted as a bias in SODA_XP if we assume HadISST1.1 is the closest to "truth". The differences are more likely to be a function of a large ensemble spread. Given that HadISST1.1 is only a single realization, there is not an easy way to determine where "truth" lies among SODA_XP's 56 members.

3.2 Inter versus Intra variability

To further examine the variability displayed in such a large ensemble set, the 56 members for each time period are separated into 8 groups based on the original SODAsi.1 SST forcing and then averaged creating 8 SODA_XP group means. Figure 8 depicts SST anomalies of the 1918/1919 DJF average for each SODAsi.1 ensemble member. These 8 different ocean solutions were used as boundary conditions for 20CRv2 Scout 3.3.1, which then forced the 56 members of SODA_XP. Enhancing the number of ocean reanalysis ensemble members from 8 to 56 aims to address the question of if there were additional ensemble members, would there be more variability?

By way of contrast, Figure 9 shows SST anomalies of the 1918/1919 DJF average for each of the 8 SODA_XP group means. When comparing Figures 8 and 9, the first noticeable feature is how different the 8 SODA_XP group mean panels are from the 8 SODAsi.1 ensemble member panels. The difference between these two figures is the atmospheric reanalysis of 20CRv2 Scout 3.3.1, which implies that atmospheric variability is acting on the prescribed ocean state in 8 considerably different ways, ultimately arising from the 8 different SST boundary conditions of SODAsi.1.

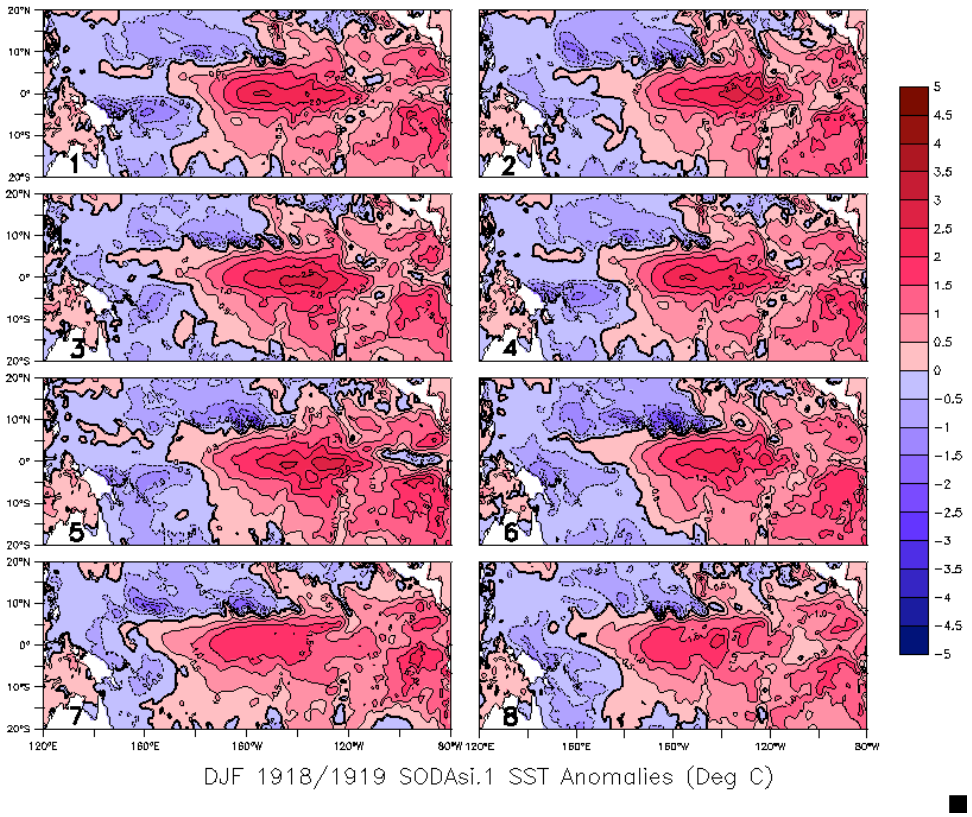

Figure 8. 1918/1919 DJF SST anomalies (°C) for SODAsi.1 ensemble members 1 through 8.

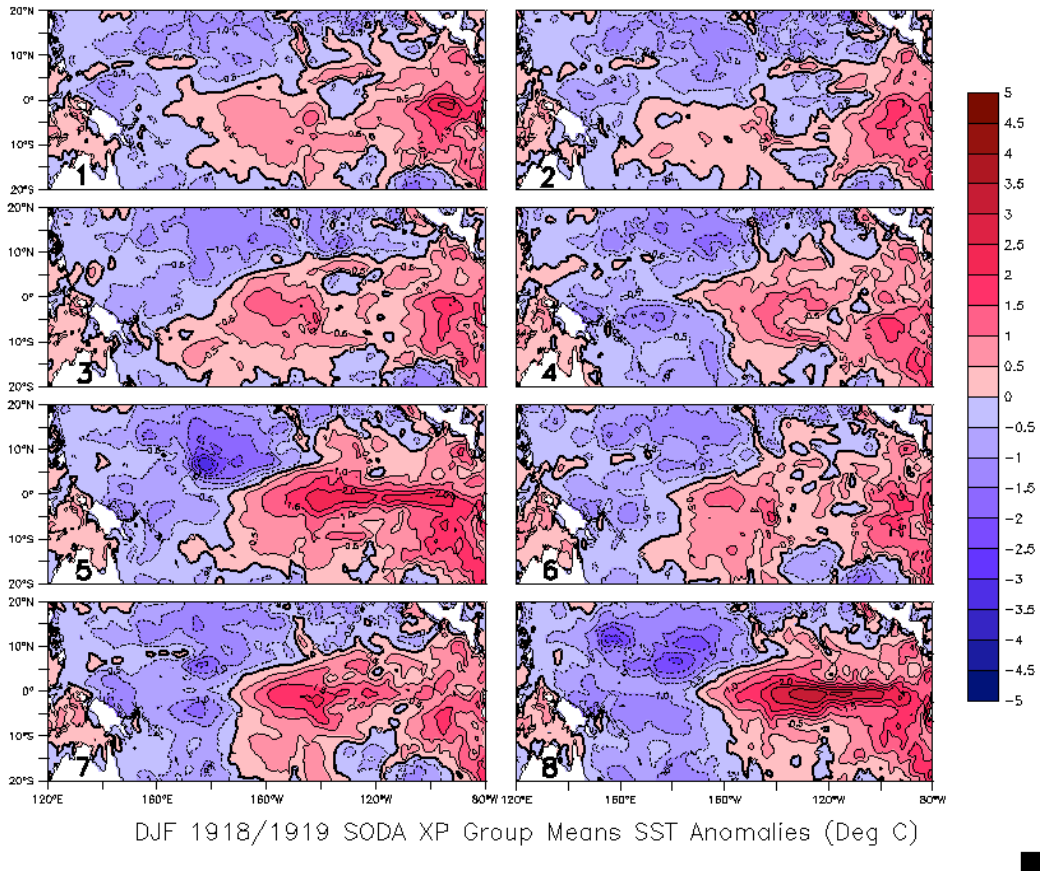

Figure 9. 1918/1919 DJF SST anomalies (°C) for SODA_XP Groups 1 through 8.

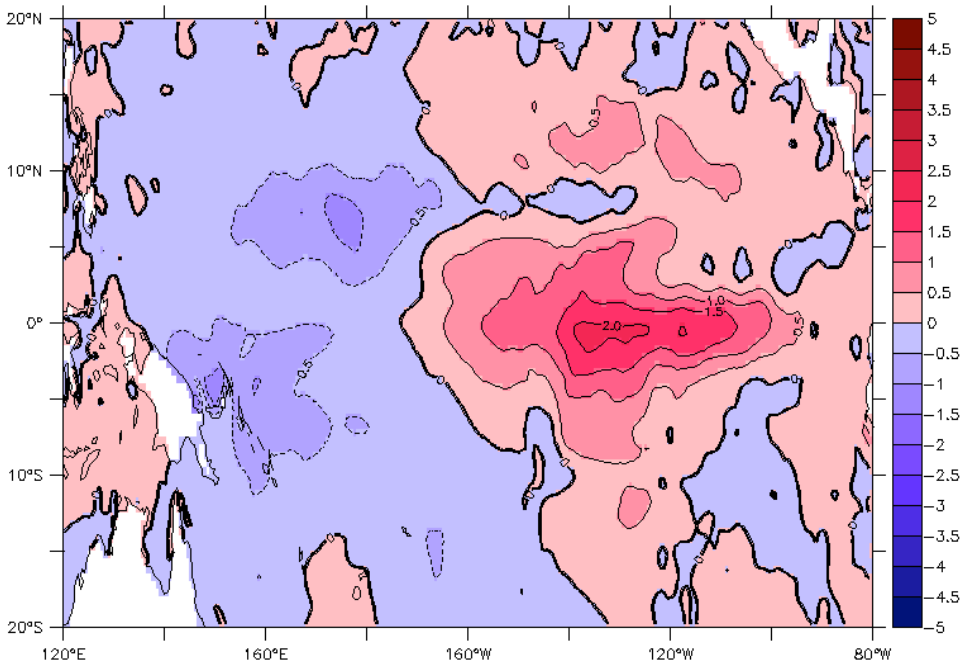

Figure 10. 1918/1919 DJF SST anomalies (°C) difference between SODA_XP Groups 2 and 8.

Analyzing the differences among groups assesses the intervariability of the reanalyses. Group 2 differenced from Group 8, shown in Figure 10, reveals the greatest difference in the strength of the El Niño event among the 8 SODA_XP groups. In fact, the magnitude of the difference between Groups 2 and 8 is comparable to that of an El Niño. This supports the proposed hypothesis that if ensemble members are forced with different estimates of SODAsi.1 SST, then the resulting SODA_XP members will yield different results. Intra-variability is also evaluated by comparing solutions of the El Niño event within each SODA_XP group among the 7 individual ensemble members. The 7 individual ensemble members of Groups 2 and 8 are shown in Figures 11 and 12.

Congruent with the intervariability findings, similarities of results within each SODA_XP group generated with the same SODAsi.1 SST suggest that atmospheric state estimates are strongly dependent upon the SST boundary condition.

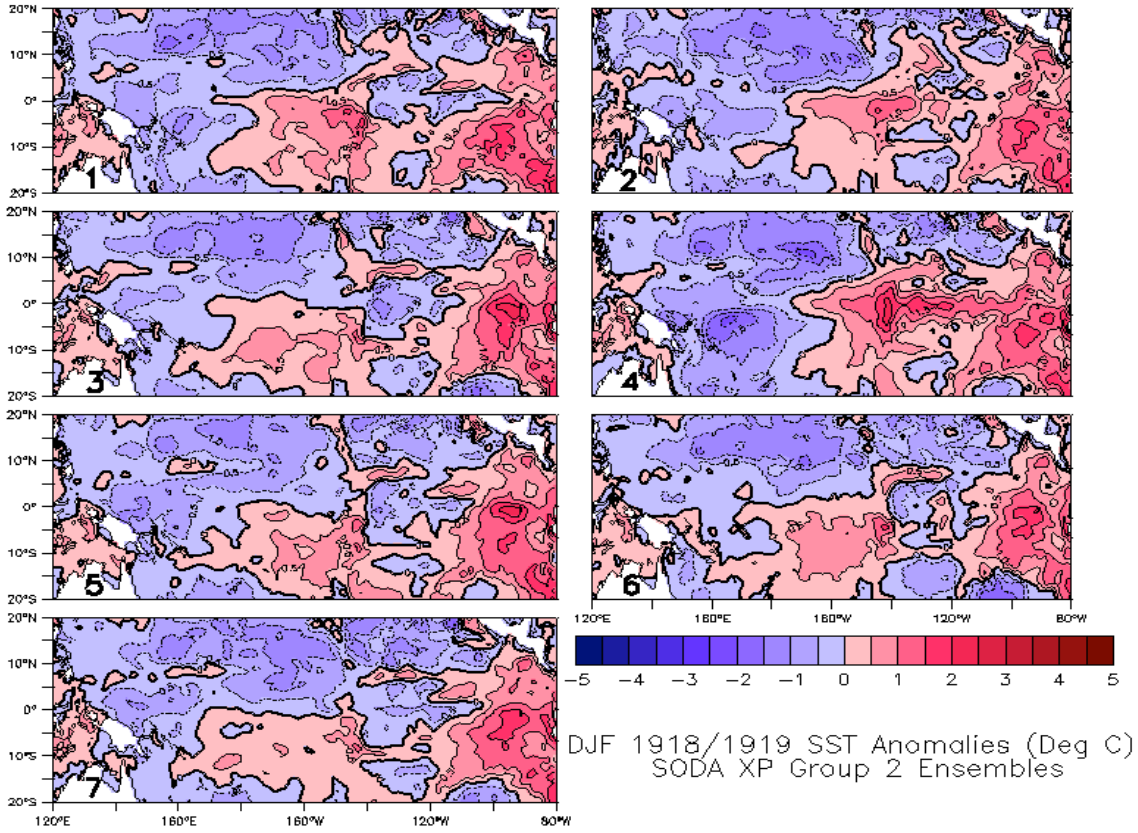

Figure 11. 1918/1919 DJF SST anomalies (°C) for the 7 ensemble members of SODA_XP Group 2.

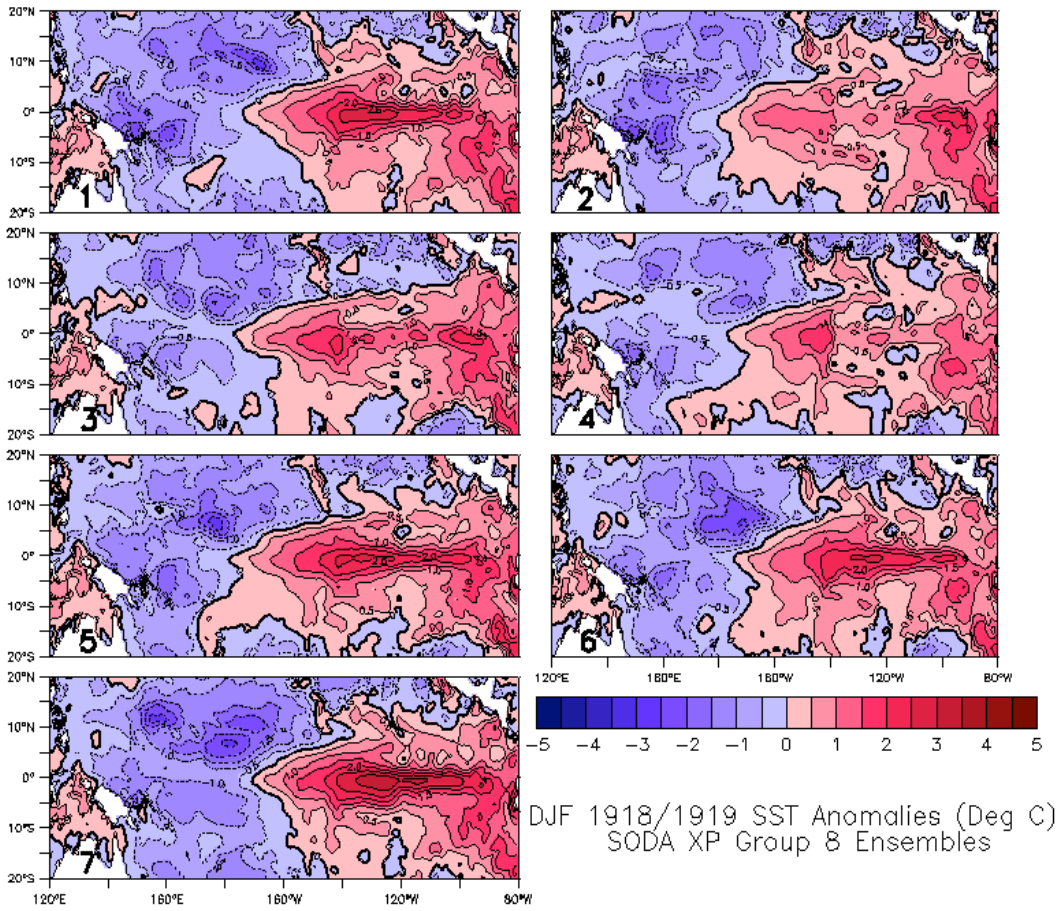

Figure 12. 1918/1919 DJF SST anomalies (°C) for the 7 ensemble members of SODA_XP Group 8.

Conversely, when looking more closely at the 7 individual ensemble members that comprise each SODA_XP group, there are differences seen as well. For example, number 4 looks more like the composite of Group 2 than Group 8. Due to the fact that these atmospheric ensemble members were all forced with the same SODAsi.1 SST, it is assumed the observed variability within in a group results from atmospheric variability within the atmospheric reanalysis. Shown in Figures 13 and 14 are examples of the

equatorial zonal wind stress maximum anomalies for the 7 ensemble members of Group 4 and Group 8 from the full 1916-1920 period. (Additional figures for the other SODA_XP groups are found in Appendix I). The high frequency bursts are random, which is characteristic of atmospheric forcing. On the other hand, the low frequency signal among all 7 ensemble members within a group follows a similar pattern. This suggests that the observed atmospheric noise has both a random attribute as well as a low frequency response to SODAsi.1 SST forcing.

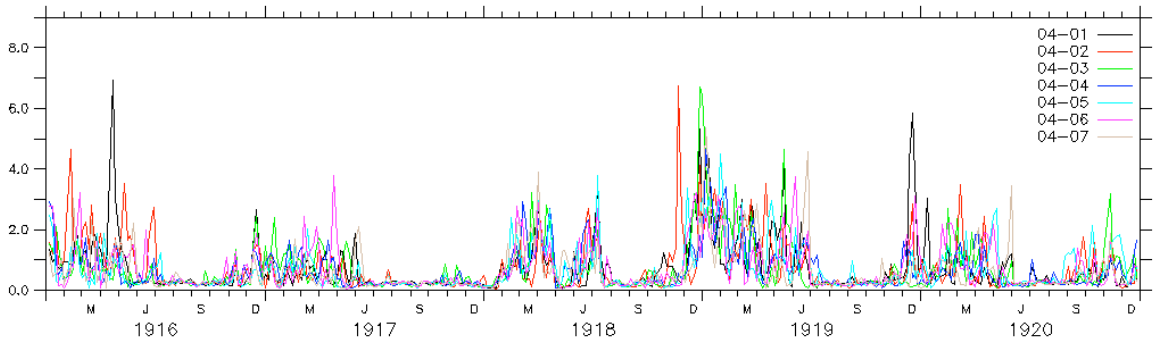

Figure 13. Equatorial zonal wind stress maximum anomalies (N/m^2) for the 7 ensemble members of Group 4 from 1916-1920. The maximum is found by searching for the maximum value from 120E to 70W at each time step.

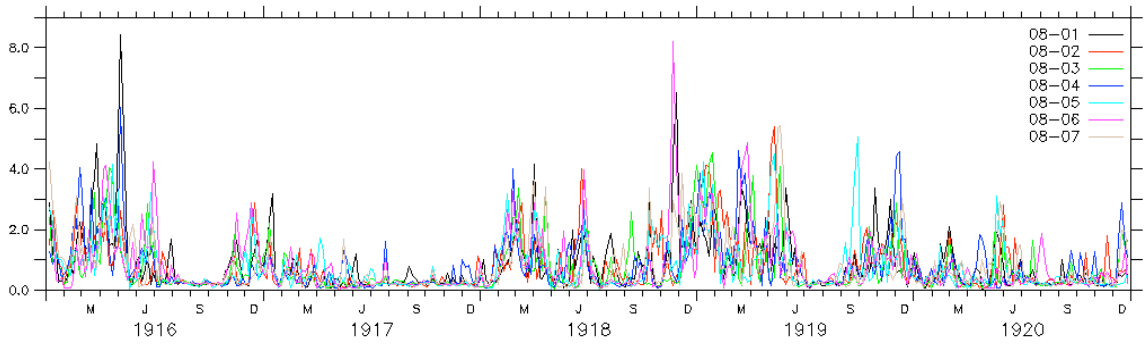

Figure 14. Equatorial zonal wind stress maximum anomalies (N/m^2) for the 7 ensemble members of Group 8 from 1916-1920.

A parallel result is found when comparing Niño3.4 SST anomalies across and within groups. Differences within a group of ensemble members forced with the same SODAsi.1 SST result from atmospheric noise affecting the ocean. Figure 15 illustrates a large ensemble spread within a group, which is present from the random atmospheric forcing feeding back on the ocean. However, these individual members generally follow a similar low frequency pattern, shown via the group mean (thicker red and blue lines). This supports the notion that low-frequency atmospheric forcing acting on the ocean is dependent upon the original SODAsi.1 SST estimate. Differences across groups are larger and more significant, thus emphasizing the role of SST forcing for atmospheric reanalyses.

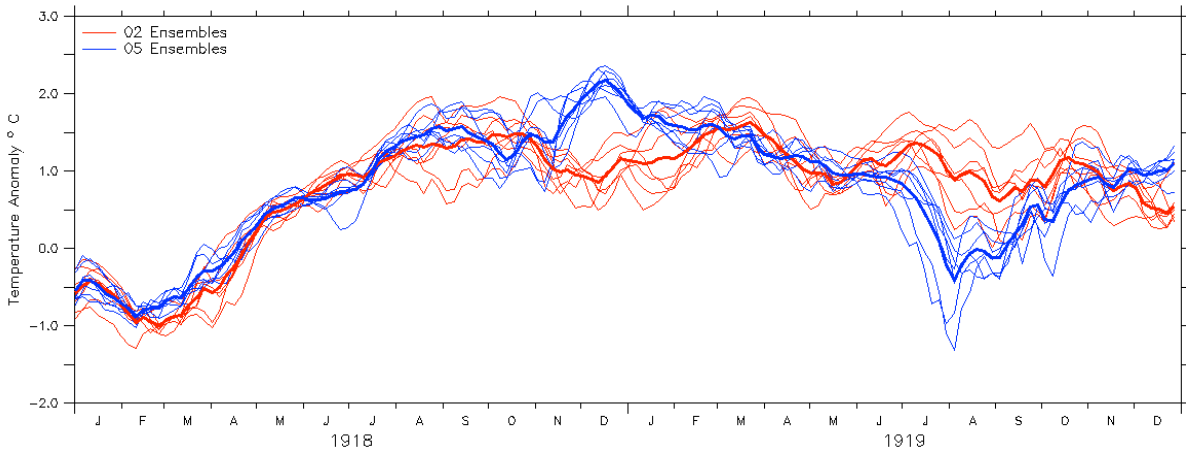

Figure 15. 1918/1919 Niño3.4 SST anomalies (°C) for SODA_XP Groups 2 and 5 from January 1918 through December 1919.

To better quantify the differences among and within SODA_XP groups, mean standard deviation of ensemble members are calculated. The standard deviation among the 7 ensemble members within a SODA_XP group is computed. These 8 standard deviation values for each SODA_XP group are then averaged over the 8 groups, which results in the total mean standard deviation. The top panel of Figure 16, is the mean standard deviation of ensembles when averaged over the 8 SODA_XP groups forced with the same SODAsi.1 SST. The bottom panel was constructed using the same procedure, except the individual ensemble members are grouped randomly instead of basing it on same SST forcing. Comparing the top panel to the bottom panel reveals less variance when averaged over SODA_XP groups than when averaged over random groups. Again, within a SODA_XP group the individual ensemble members are more similar to each other implying that there is a deterministic feature to the original SODAsi.1 SST estimates.

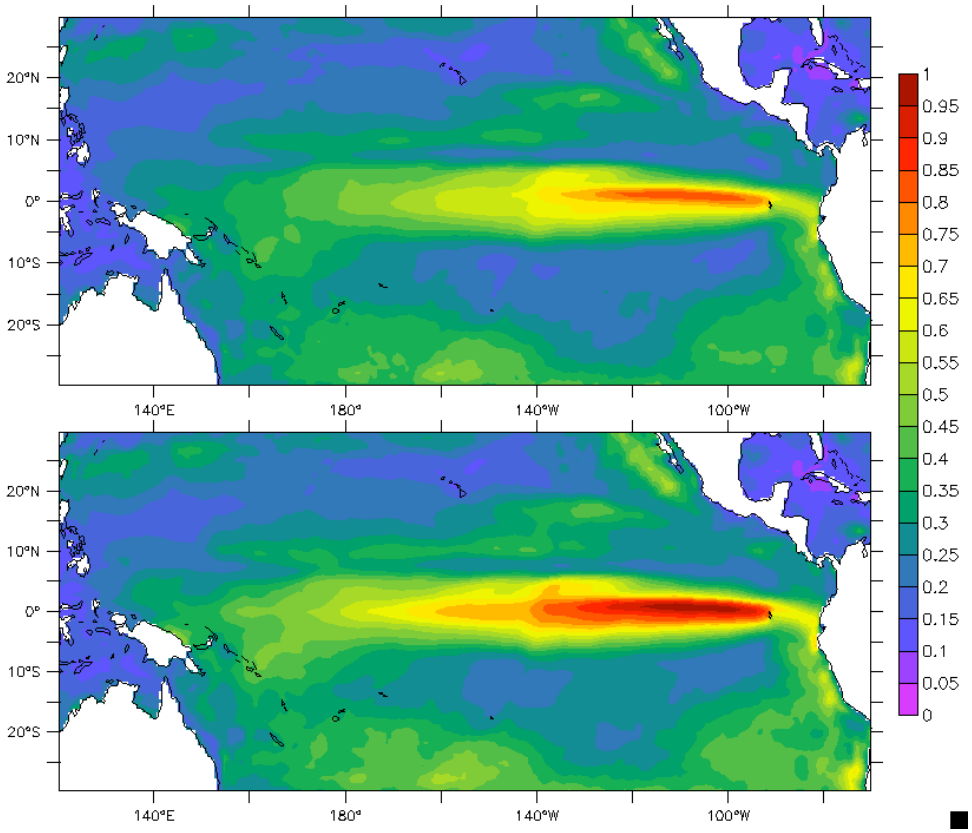

Figure 16. Standard deviation of ensembles for SST (°C) in the Tropical Pacific averaged over SODA_XP groups (top) and randomly assembled groups (bottom) from 1916-1920.

These results are investigated further with Figure 17, which shows 8 red lines for SODA_XP group mean SST and 8 blue lines for randomly assembled group mean SST from 1916-1920 and 1996-2000. Both have the total 56 member ensemble mean subtracted to calculate the anomaly field. The 8 randomly grouped blue lines show a much smaller range of values from -0.20°C to 0.20°C. Conversely, the red lines represent grouped means and show a larger range of -1.20°C to 0.80°C. By subtracting the 56 member ensemble mean from these grouped and random means, both high and low frequency signals become more apparent. The high frequency atmospheric noise is

present in all curves, and is the dominant feature for the random means. Low frequency noise, which results from the atmosphere's response to original SODAsi.1 forcing, is significantly more visible in the grouped means. In fact, the difference in ranges between the group means and the randomly assembled group means gives a direct quantity of how much feedback the atmosphere reanalysis experienced from the SODAsi.1 forcing, which then reflects back in the iteration of SODA_XP fields. Moreover, groups of ensembles forced with the same SODAsi.1 SST estimates do not show a normal distribution about the mean. However, random groups of ensembles forced with different SODAsi.1 SST estimates are normally distributed because they only represent the random atmospheric noise present.

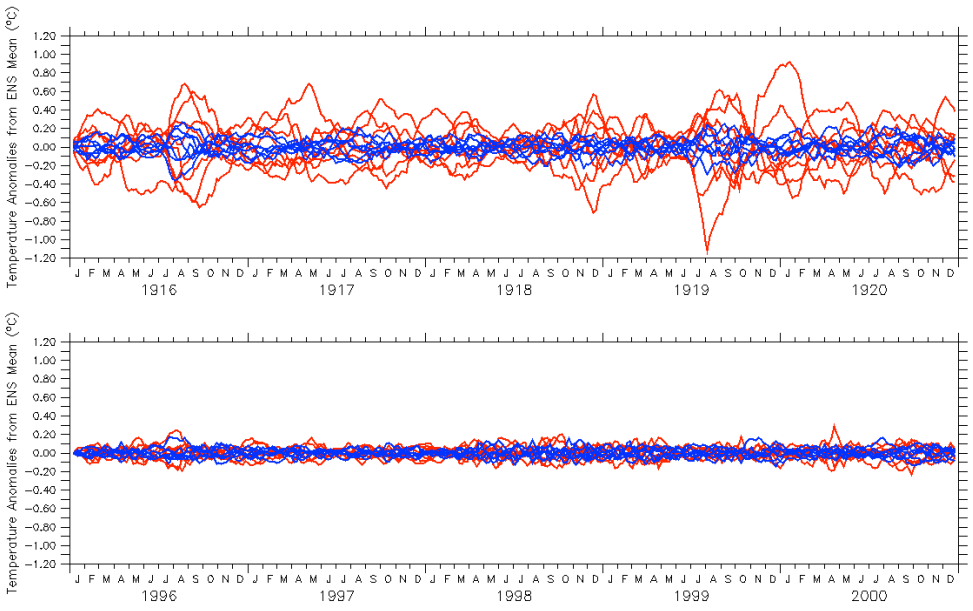

Figure 17. SODA_XP 8 group mean SST (red) and 7 random group mean SST (blue) from 1916-1920 (top) and 1996-2000 (bottom). These anomalies are calculated by subtracting the 56 ensemble member mean from both grouped and randomly assmebled means.

3.3 1997/1998 El Niño

In addition to the results produced from the 1916-1920 assimilation, the 1996-2000 assimilation also reveals interesting findings. The 56 member ensemble mean of zonal wind stress and SST are shown in Figure 18. The left hand panel depicts some WWBs preceding the El Niño event, but there are few high frequency bursts of energy once the SST anomaly grew in strength. Comparing these results to those of the earlier period (Figure 4), the high frequency wind anomalies seem to be more constrained to the beginning of the 1997/1998 El Niño event rather than persisting throughout, as seen in the El Niño of 1918/1919. Again, these wind anomalies are expected in individual members of a large ensemble set, but since they persist in an ensemble mean of all 56 ensembles, it suggests they remain an important variable to consider when analyzing the initial formation of an El Niño event.

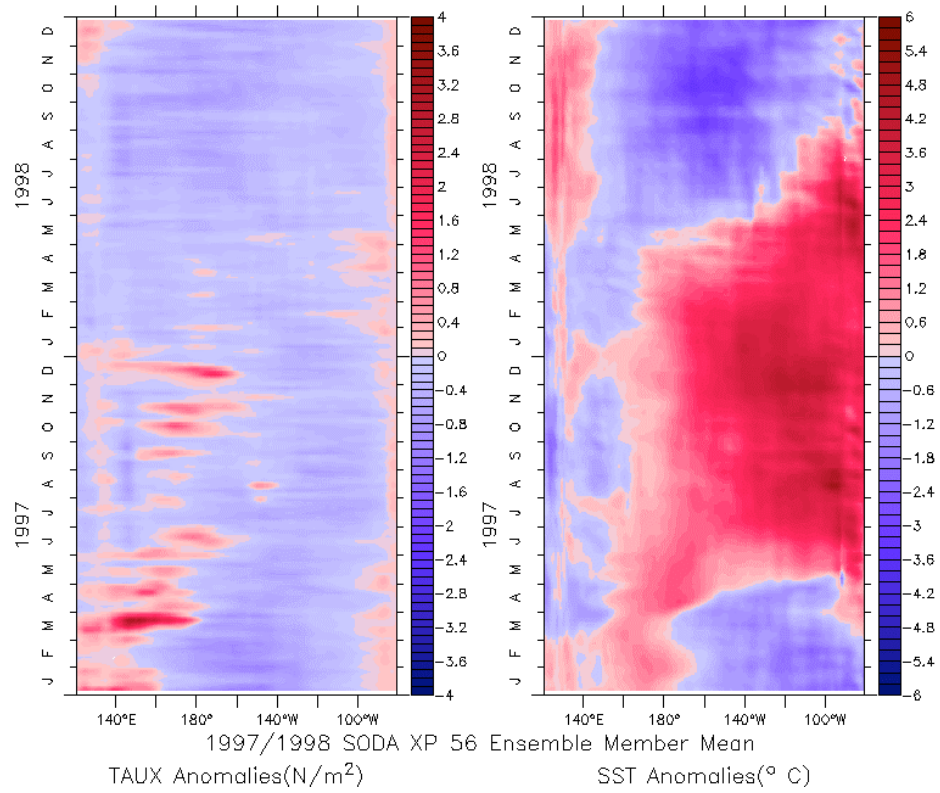

Figure 18. Zonal wind stress (N/m^2) (left panel) and SST (°C) (right panel) anomalies of the 56 ensemble mean for 1996 – 2000.

The bottom panel of Figure 17 contains 8 group mean lines and 7 random grouped lines for Niño3.4 SST anomaly from the 56 ensemble member mean for 1996-2000. The time series for 1996-2000 is markedly different from the earlier period. Of considerable importance is how much the range of the grouped means (red lines) decreases between the two time periods. In fact, the group means and the random group means do not seem to vary much at all, which suggests that the greater availability of observations for assimilation in the later period greatly decreases the range of the ensemble spread. The same findings are seen in Figures 19 and 20 where the SODA_XP

ensemble members encompass a much smaller range in variability of the SST estimate. Comparing Figure 19 with Figure 7, there is considerably less uncertainty in the estimation of the ocean state in 1996-2000. Most of the variance seen is derived from atmospheric noise for both grouped means and randomly grouped means.

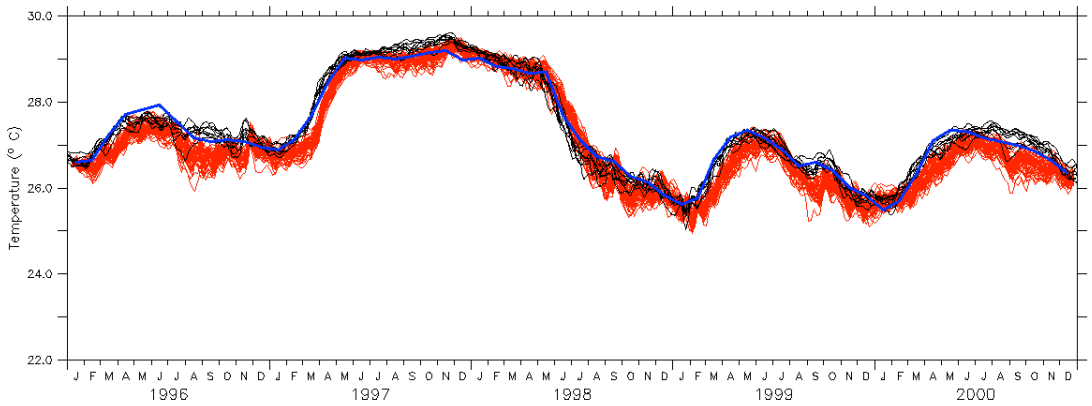

Figure 19. Niño3.4 SST (°C) for HadISST1.1 (blue), SODAsi.1 8 ensembles (black), and SODA_XP 56 ensembles (red) from 1996-2000.

When looking more closely at the individual group means and the ensemble members that comprise those groups, the ensemble spread decreases within groups. Figure 20 shows the Niño3.4 SST anomaly from SODA_XP Groups 2 and 5. All of the ensemble members within both groups show strong agreement, and the same is true between both of the group means (thicker lines). These results are expected when analyzing a heavily observed period because of the decrease in uncertainty associated with assimilating more observations. Furthermore, the variance of the ensemble spread

for 1996-2000 shows less variance for both group means and randomly grouped means as shown in Figure 21. There is a slight difference between group means and randomly grouped means on the order of 0.01°C^2; this supplements previous results indicating that uncertainty in the 1996-2000 SST estimate is negligible, and any observed variance is attributed to atmospheric noise.

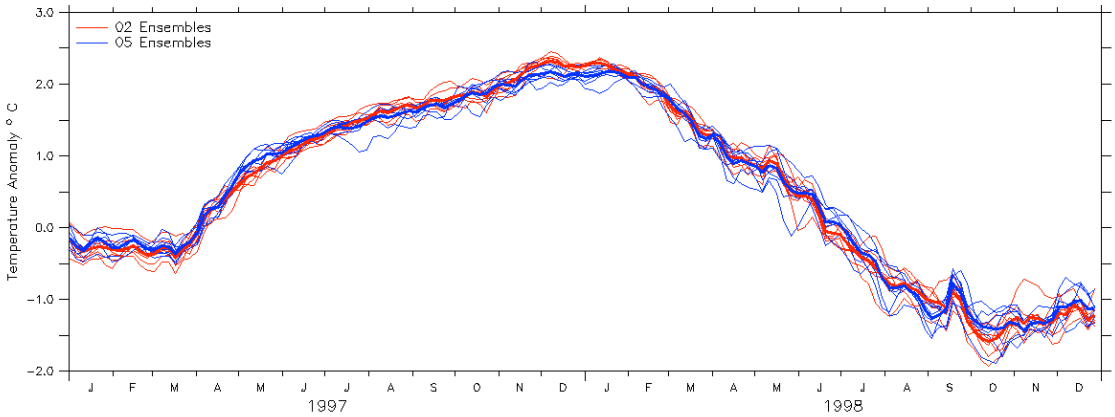

Figure 20. 1918/1919 Niño3.4 SST anomalies (°C) for SODA_XP Groups 2 and 5 from January 1997 through December 1998.

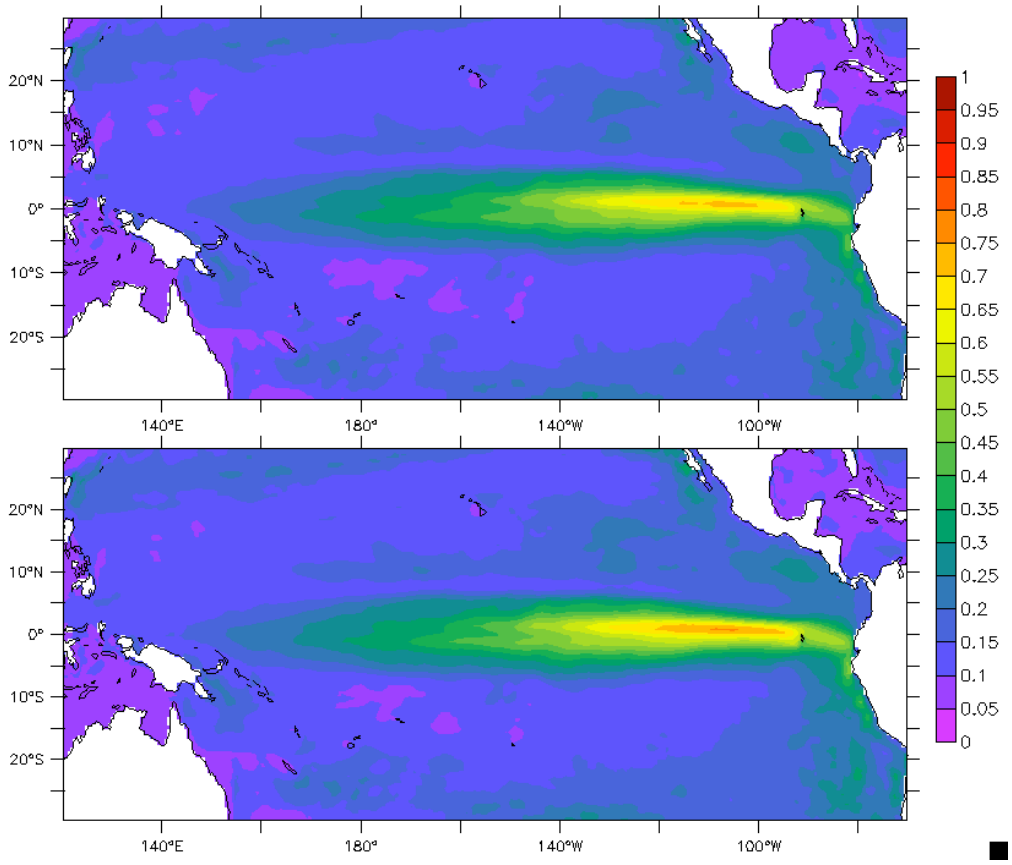

Figure 21. Standard deviation of ensembles for SST (°C) in the Tropical Pacific averaged over SODA_XP groups (top) and randomly assembled groups (bottom) from 1996-2000.

4. SUMMARY AND CONCLUSIONS

Results from four experiments each characterized by a 56-member ensemble of ocean reanalyses are presented. The project, collectively called SODA_XP, covers two 5-year periods, 1916-1920 and 1996-2000, with both assimilation and simulation products. Generation of the atmospheric forcing fields was performed using a 56 member atmospheric reanalysis system (20CRv2) with oceanic boundary conditions of 8 different SST estimates from SODAsi.1. These reanalyses are part of an overall effort to run reanalyses iteratively in an effort to improve state estimates of the ocean and atmosphere during periods of sparse observations, as well as to emphasize the importance of loosely coupling ocean and atmosphere reanalyses.

The results show there are two sources of uncertainty in the reanalyses. One comes from inherent atmospheric noise, and is largely constant through time, even as the number of observations grows. The other source comes from uncertainty in prescribing SST to the atmosphere. This is markedly reduced as the number of observations increases in later periods. This alone is strong evidence that a coupled reanalysis system is required to adequately represent the range of possible climate states in periods of few observations.

The SODA_XP SST fields highlighting the 1918/1919 El Niño show a wide range of variability in terms of strength, duration, and location among the 56 ensemble members. In contrast, all ensembles show general agreement for the 1997/1998 El Niño. High frequency zonal wind anomalies, or WWB, are observed in both of the 56

ensemble member means indicating that they are important to consider when analyzing an El Niño event. After dividing SODA_XP into 8 groups based on the original SODAsi.1 ensemble used as forcing for 20CRv2, the 1918/1919 El Niño appears to have the most intervariability between Groups 2 and 8. Differences among groups are attributed to variations in the 8 ocean state estimates from SODAsi.1 that were used as forcing for 20CRv2. However, there is also intravariability present within the 7 ensemble members of a group. The intravariability is characteristic of both random atmospheric noise as well as the variance associated with the atmosphere responding to the original ocean forcing. As expected, there is little variance seen among members for the 1997/1998 El Niño as both the ocean and atmosphere reanalyses are more constrained by observations.

Comparable results concerning intravariability between the two periods conclude that atmospheric forcing makes a difference in how SODAsi resolves an ENSO event. It is clear that the ocean is sensitive to the ensemble forcing of the atmosphere from both randomly generated atmospheric noise and the atmospheric response to the ocean forcing. Likewise, similarities of results within each SODA_XP group generated with the same SODAsi.1 SST suggest that atmospheric state estimates are strongly dependent upon the SST boundary condition. On the whole, all of the presented results suggest that coupling reanalysis between the ocean and atmosphere is important when examining phenomenon such as ENSO. Future work in this area will include another iteration to analyze convergence of results. Additionally, constructing a fully coupled climate model

with data assimilation would be most beneficial to better resolve phenomena associated with air-sea interactions.

REFERENCES

Bjerknes, J. (1969), Atmospheric teleconnections from the equatorial Pacific, *Monthly Weather Review*, *97*(3), 163-172.

Brönnimann, S., G. P. Compo, R. Spadin, R. Allan, and W. Adam (2011), Early ship-based upper-air data and comparison with the twentieth century reanalysis, *Climate of the Past*, *7*(1), 265-276.

Brönnimann, S., A. Grant, G. Compo, T. Ewen, T. Griesser, A. Fischer, M. Schraner, and A. Stickler (2012), A multi-data set comparison of the vertical structure of temperature variability and change over the Arctic during the past 100 years, *Climate Dynamics*, *39*(7-8), 1577-1598.

Carton, J. A., and B. S. Giese (2008), A reanalysis of ocean climate using Simple Ocean Data Assimilation (SODA), *Monthly Weather Review*, *136*(8), 2999-3017.

Chavez, F. P., M. Messié, and J. T. Pennington (2011), Marine primary production in relation to climate variability and change, *Annual Review of Marine Science*, *3*(1), 227-260.

Compo, G. P., J. S. Whitaker, and P. D. Sardeshmukh (2006), Feasibility of a 100-year reanalysis using only surface pressure data, *Bulletin of the American Meteorological Society*, *87*(2), 175-190.

Compo G. P., J. S. Whitaker, P. D. Sardeshmukh, N. Matsui, R. J. Allan, X. Yin, B. E. Jr. Gleason, R. S. Vose , G. Rutledge, P. Bessemoulin, S. Brönnimann, M. Brunet, R.I. Crouthamel, A. Grant, P. Y. Groisman, P. D. Jones, M. C. Kruk, A. C. Kruger, G. J. Marshall, M. Maugeri, H. Y. Mok, Ø. Nordli, T. F. Ross, R. M. Trigo, X. L. Wang, S. D. Woodruff, and S. J. Worley (2011), The twentieth century reanalysis project, *Q. J. R. Meteorol. Soc., 137*, 1–28.

Compo, G. P., P. D. Sardeshmukh, J. S. Whitaker, P. Brohan, P. D. Jones, and C. McColl (2013), Independent confirmation of global land warming without the use of station temperatures, *Geophysical Research Letters*, *40*(12), 3170-3174.

Giese, B. S., N. C. Slowey, S. Ray, G. P. Compo, P. D. Sardeshmukh, J. A. Carton, and J. S. Whitaker (2010), The 1918/19 El Niño, *Bulletin of the American Meteorological Society*, *91*(2), 177-183.

Giese, B. S., and S. Ray (2011), El Niño variability in Simple Ocean Data Assimilation (SODA), 1871–2008, *Journal of Geophysical Research: Oceans*, *116*(C2), C02024.

Jones, P. W. (1999), First- and second-order conservative remapping schemes for grids in spherical coordinates, *Monthly Weather Review*, *127*(9), 2204-2210.

Kaplan, A., M. A. Cane, Y. Kushnir, A. C. Clement, M. B. Blumenthal, and B. Rajagopalan (1998), Analyses of global sea surface temperature 1856–1991, *Journal of Geophysical Research: Oceans*, *103*(C9), 18567-18589.

Rasmusson, E. M., and J. M. Wallace (1983), Meteorological aspects of the El Niño/Southern Oscillation, *Science*, *222*(4629), 1195-1202.

Ray, S., and B. S. Giese (2012), Historical changes in El Niño and La Niña characteristics in an ocean reanalysis, *Journal of Geophysical Research: Oceans*, *117*(C11), C11007.

Rayner, N. A., D. E. Parker, E. B. Horton, C. K. Folland, L. V. Alexander, D. P. Rowell, E. C. Kent, and A. Kaplan (2003), Global analyses of sea surface temperature, sea ice, and night marine air temperature since the late nineteenth century, *Journal of Geophysical Research: Atmospheres*, *108*(D14).

Schubert, S. D., M. J. Suarez, P. J. Pegion, R. D. Koster, and J. T. Bacmeister (2004), On the cause of the 1930s Dust Bowl, *Science*, *303*(5665), 1855-1859.

Seager, R., Y. Kushnir, C. Herweijer, N. Naik, and J. Velez (2005), Modeling of tropical forcing of persistent droughts and pluvials over western North America: 1856–2000*, *Journal of Climate*, *18*(19), 4065-4088.

Smith, R. D., J. K. Dukowicz, and R. C. Malone (1992), Parallel ocean general circulation modeling, *Physica D: Nonlinear Phenomena*, *60*(1–4), 38-61.

Smith, T. M., R. W. Reynolds, T. C. Peterson, and J. Lawrimore (2008), Improvements to NOAA's historical merged land–ocean surface temperature analysis (1880–2006), *Journal of Climate*, *21*(10), 2283-2296.

Vecchi, G. A., and B. J. Soden (2007), Effect of remote sea surface temperature change on tropical cyclone potential intensity, *Nature*, *450*(7172), 1066-1070.

Walker, G.T. (1924), Correlation in seasonal variations of weather, IX: A further study of world weather, *Memoirs of the India Meteorological Department, 24*, (9), 275-333.

Whitaker, J. S., and T. M. Hamill (2002), Ensemble data assimilation without perturbed observations, *Monthly Weather Review*, *130*(7), 1913-1924.

Whitaker, J. S., G. P. Compo, X. Wei, and T. M. Hamill (2004), Reanalysis without radiosondes using ensemble data assimilation, *Monthly Weather Review*, *132*(5), 1190-1200.

Woodruff, S. D., et al. (2011), ICOADS Release 2.5: extensions and enhancements to the surface marine meteorological archive, *International Journal of Climatology*, *31*(7), 951-967.

Yang, C., and B. S. Giese (2013), El Niño Southern Oscillation in an ensemble ocean reanalysis and coupled climate models, *Journal of Geophysical Research: Oceans*, *118*(9), 4052-4071.

APPENDIX A

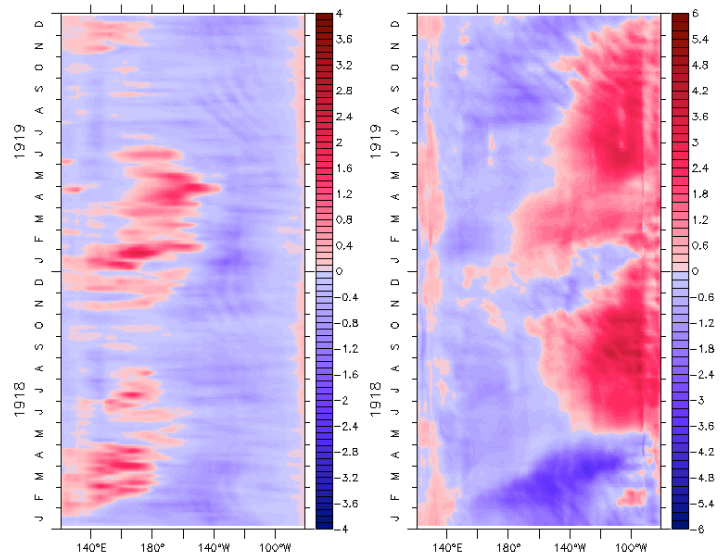

Figure A-1. Zonal wind stress (N/m^2) (left panel) and SST (°C) (right panel) anomalies of SODA_XP Group 1 from 1918 – 1919.

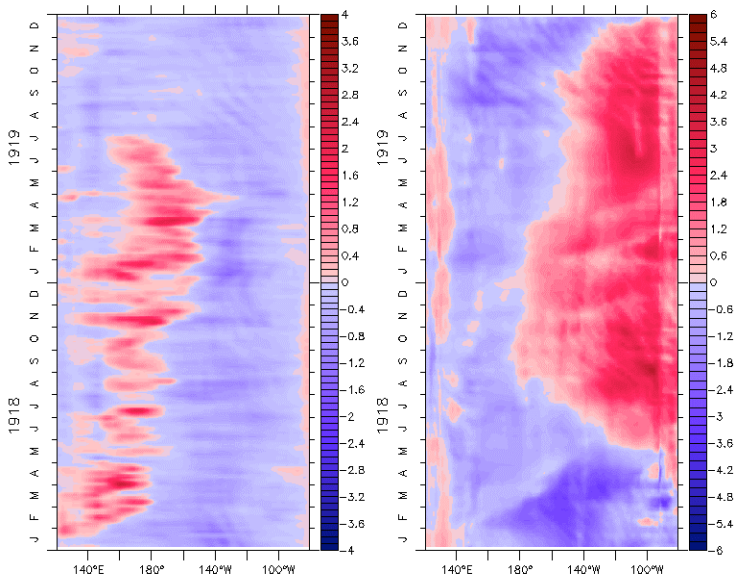

Figure A-2. Zonal wind stress (N/m^2) (left panel) and SST (°C) (right panel) anomalies of SODA_XP Group 2 from 1918 – 1919.

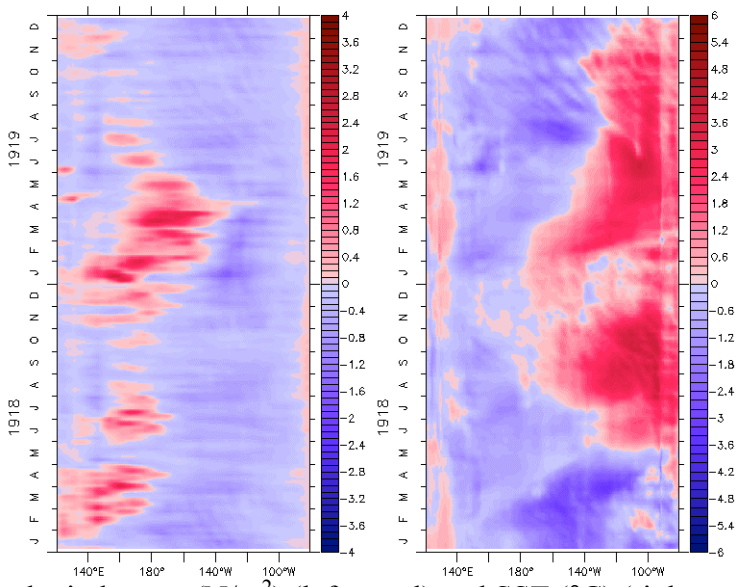

Figure A-3. Zonal wind stress (N/m^2) (left panel) and SST (°C) (right panel) anomalies of SODA_XP Group 3 from 1918 – 1919.

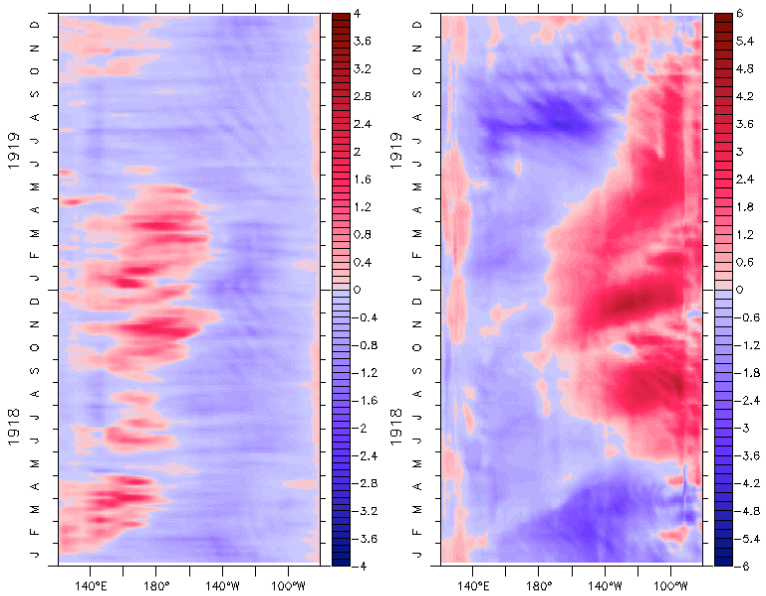

Figure A-4. Zonal wind stress (N/m^2) (left panel) and SST (°C) (right panel) anomalies of SODA_XP Group 4 from 1918 – 1919.

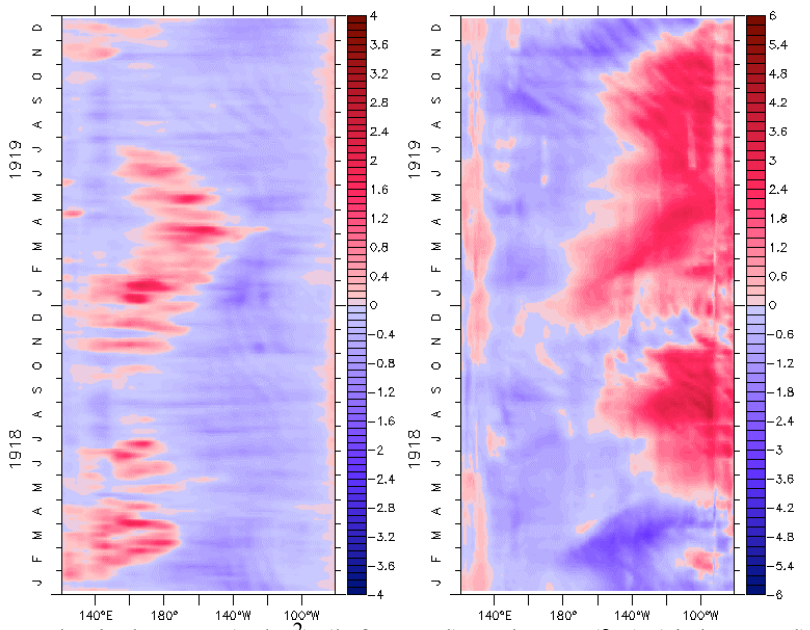

Figure A-5. Zonal wind stress (N/m^2) (left panel) and SST (°C) (right panel) anomalies of SODA_XP Group 5 from 1918 – 1919.

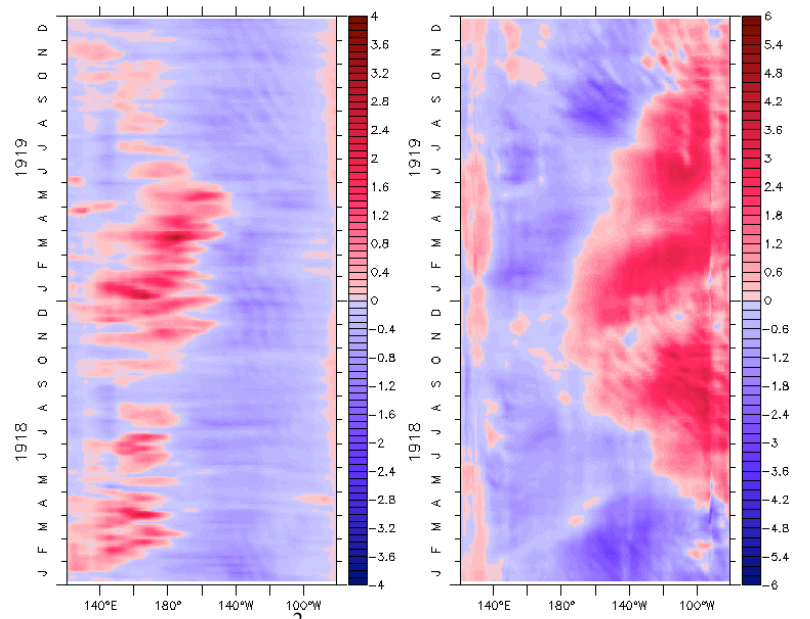

Figure A-6. Zonal wind stress (N/m^2) (left panel) and SST (°C) (right panel) anomalies of SODA_XP Group 6 from 1918 – 1919.

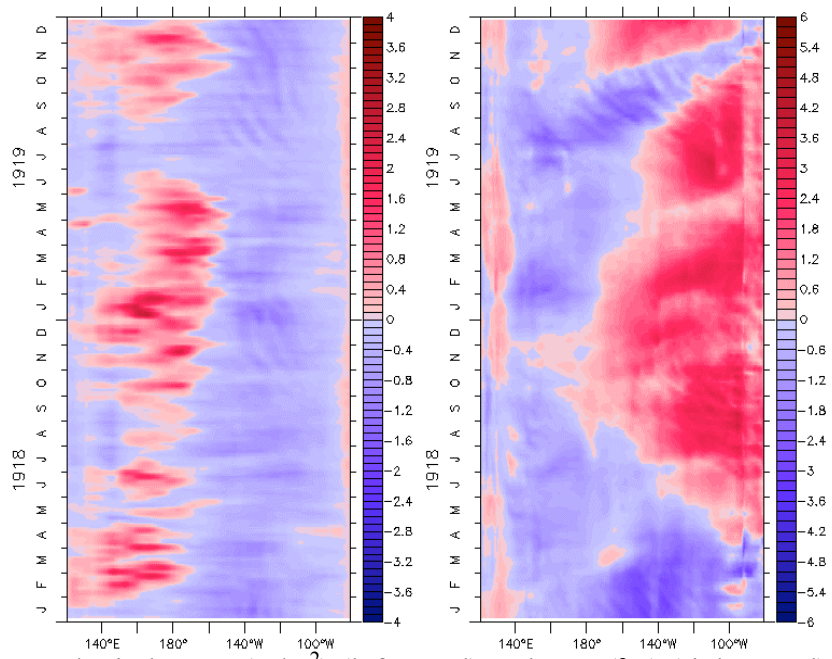

Figure A-7. Zonal wind stress (N/m^2) (left panel) and SST (°C) (right panel) anomalies of SODA_XP Group 7 from 1918 – 1919.

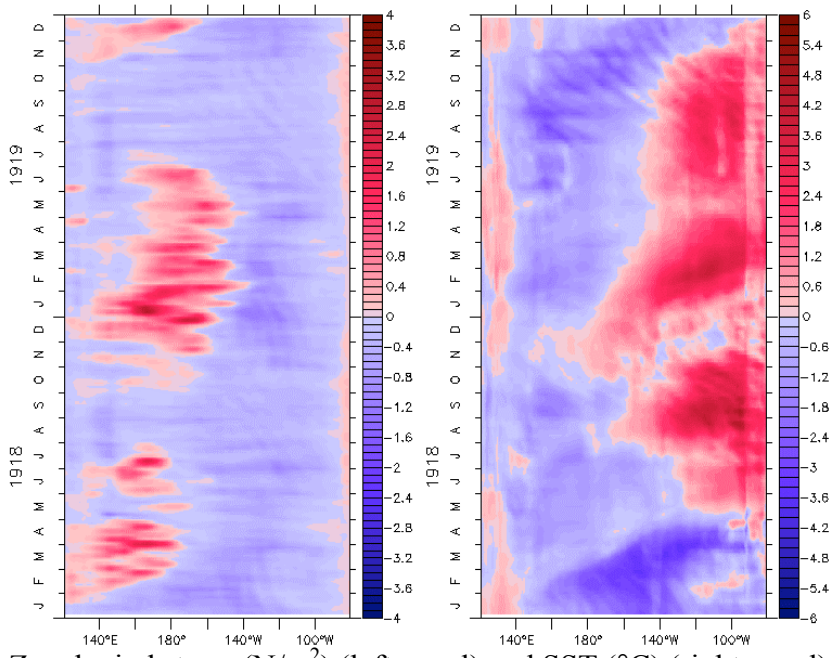

Figure A-8. Zonal wind stress (N/m^2) (left panel) and SST (°C) (right panel) anomalies of SODA_XP Group 8 from 1918 – 1919.

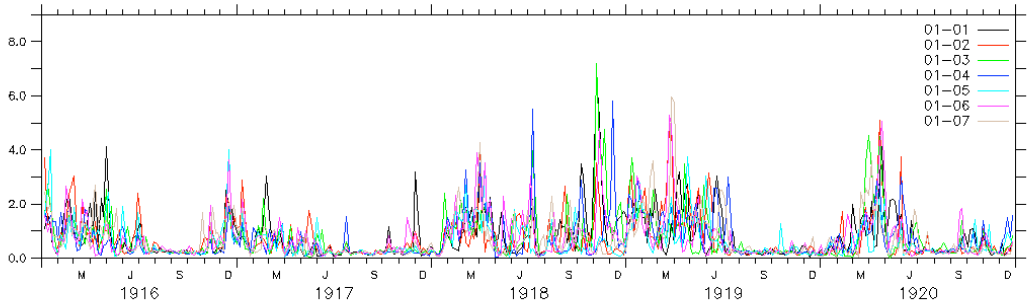

Figure A-9. Equatorial zonal wind stress maximum anomalies (N/m^2) for the 7 ensemble members of SODA_XP Group 1 from 1916-1920.

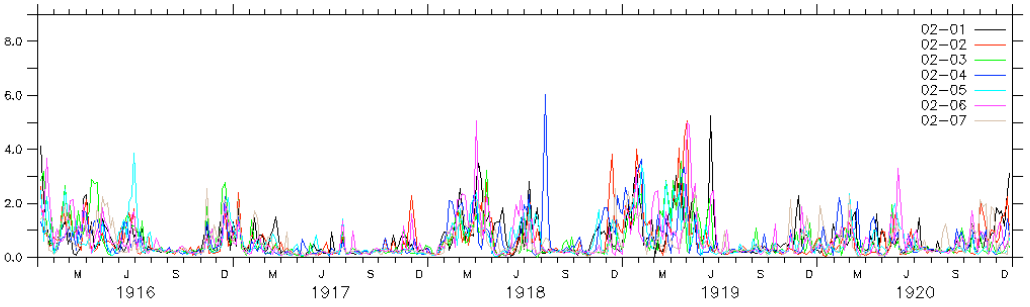

Figure A-10. Equatorial zonal wind stress maximum anomalies (N/m^2) for the 7 ensemble members of SODA_XP Group 2 from 1916-1920.

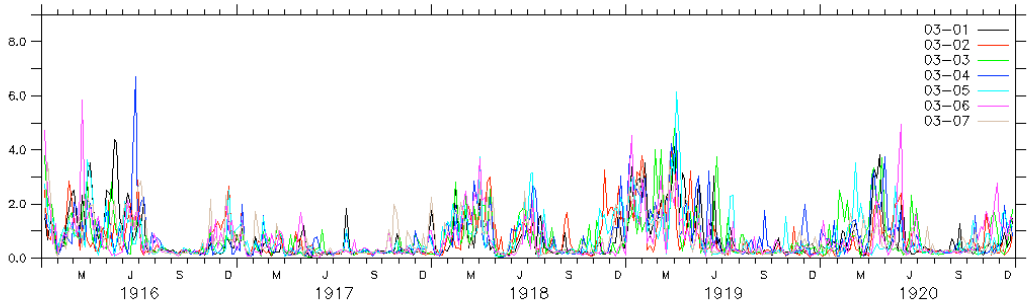

Figure A-11. Equatorial zonal wind stress maximum anomalies (N/m^2) for the 7 ensemble members of SODA_XP Group 3 from 1916-1920.

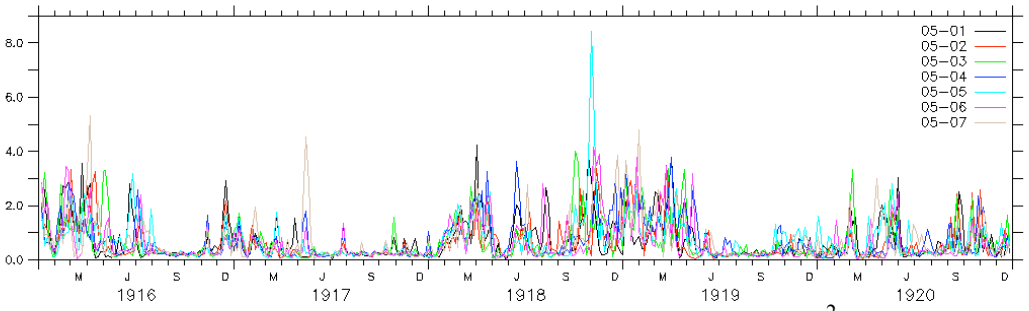

Figure A-12. Equatorial zonal wind stress maximum anomalies (N/m^2) for the 7 ensemble members of SODA_XP Group 5 from 1916-1920.

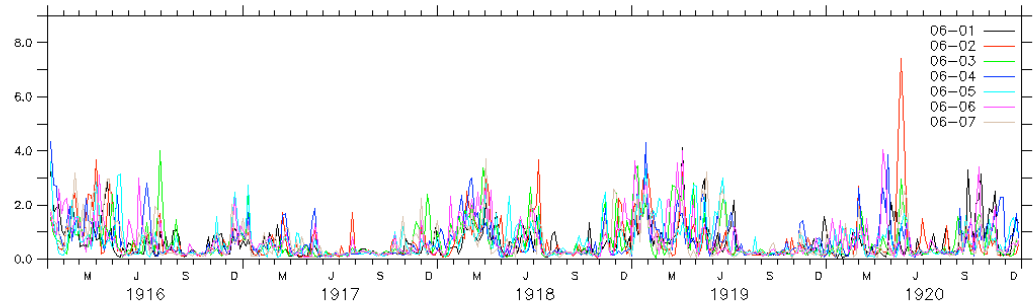

Figure A-13. Equatorial zonal wind stress maximum anomalies (N/m^2) for the 7 ensemble members of SODA_XP Group 6 from 1916-1920.

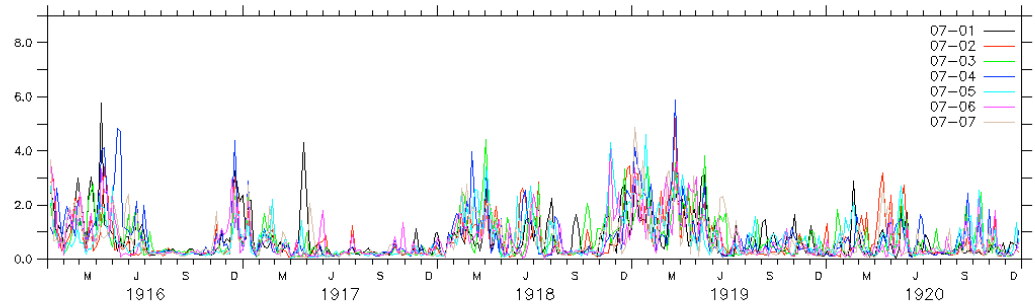

Figure A-14. Equatorial zonal wind stress maximum anomalies (N/m^2) for the 7 ensemble members of SODA_XP Group 7 from 1916-1920.

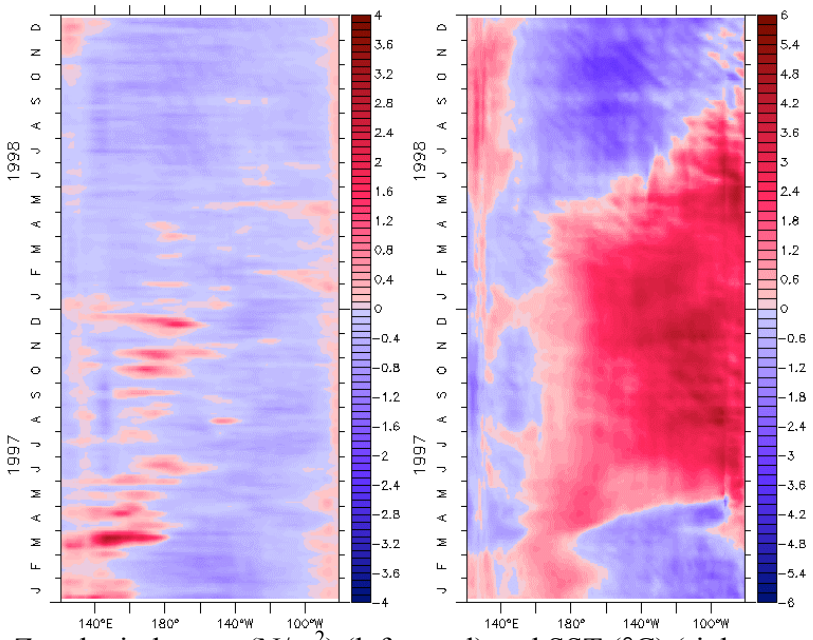

Figure A-15. Zonal wind stress (N/m^2) (left panel) and SST (°C) (right panel) anomalies of SODA_XP Group 1 from 1997 – 1998.

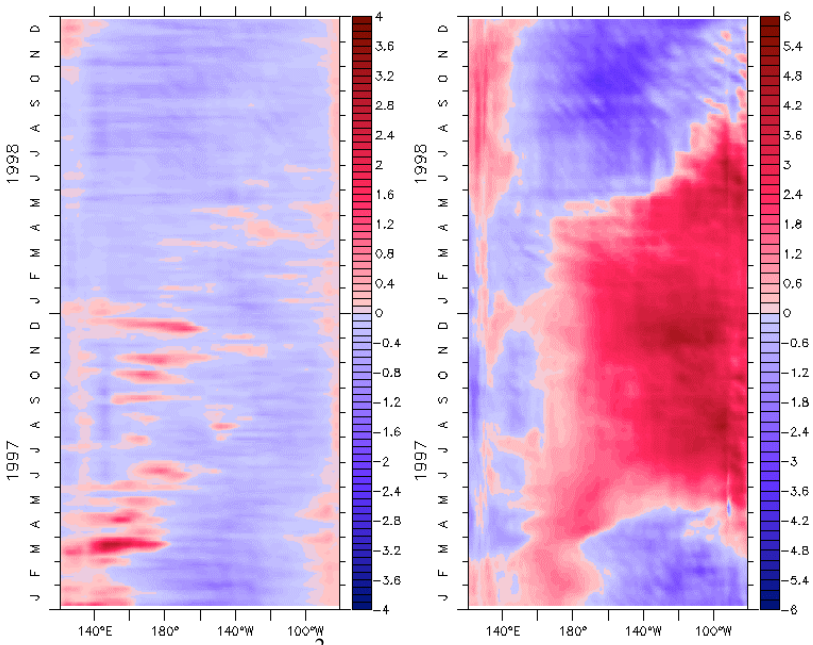

Figure A-16. Zonal wind stress (N/m^2) (left panel) and SST (°C) (right panel) anomalies of SODA_XP Group 2 from 1997 – 1998.

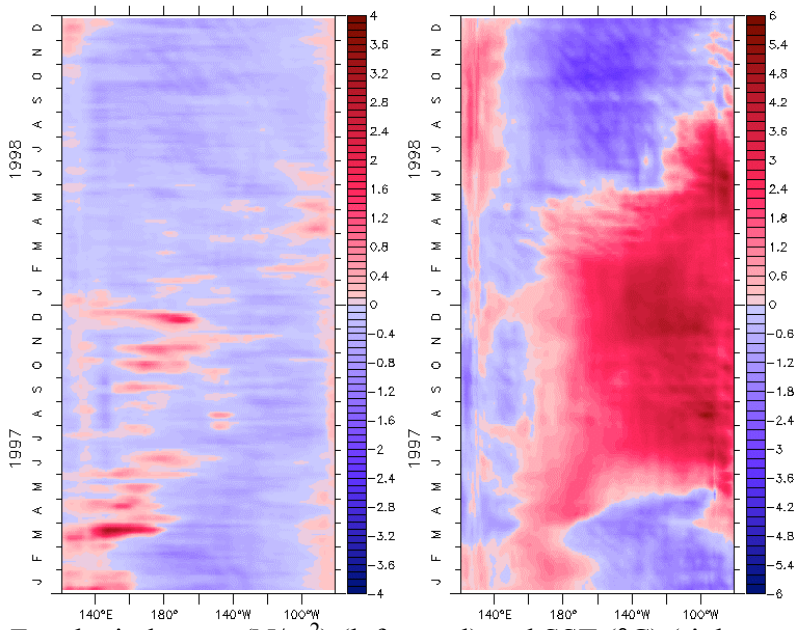

Figure A-17. Zonal wind stress (N/m^2) (left panel) and SST (°C) (right panel) anomalies of SODA_XP Group 3 from 1997 – 1998.

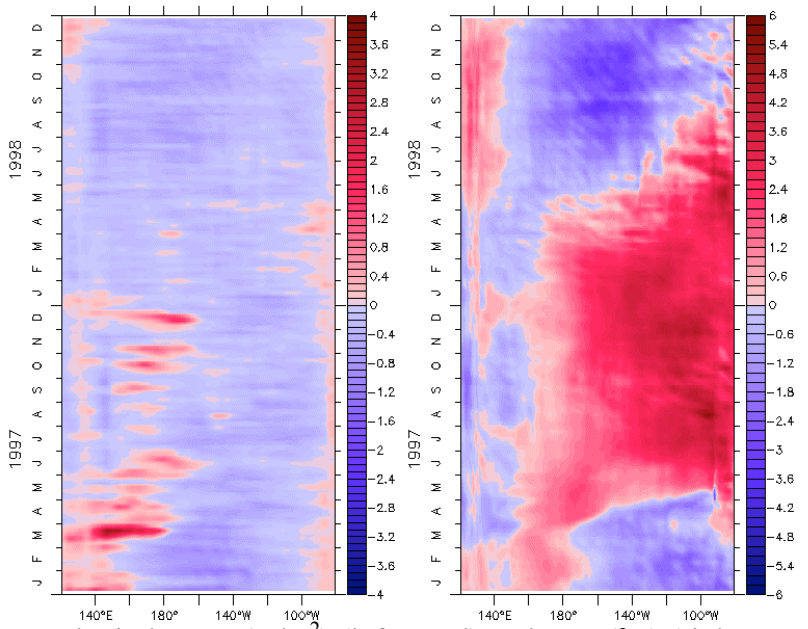

Figure A-18. Zonal wind stress (N/m^2) (left panel) and SST (°C) (right panel) anomalies of SODA_XP Group 4 from 1997 – 1998.

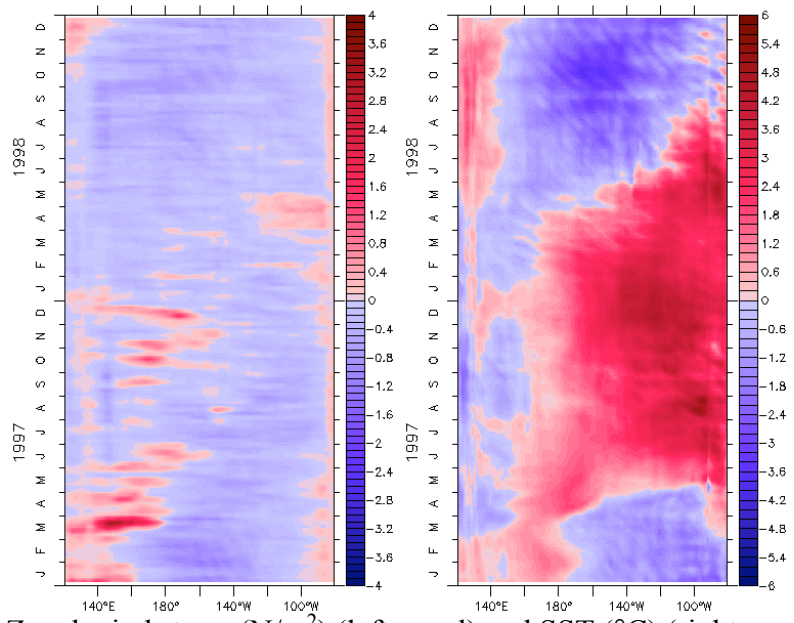

Figure A-19. Zonal wind stress (N/m^2) (left panel) and SST (°C) (right panel) anomalies of SODA_XP Group 5 from 1997 – 1998.

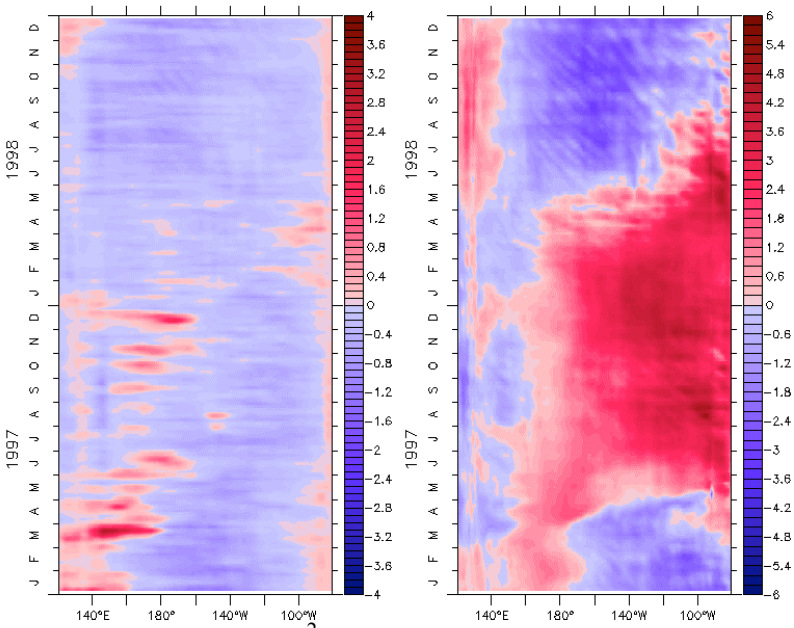

Figure A-20. Zonal wind stress (N/m^2) (left panel) and SST (°C) (right panel) anomalies of SODA_XP Group 6 from 1997 – 1998.

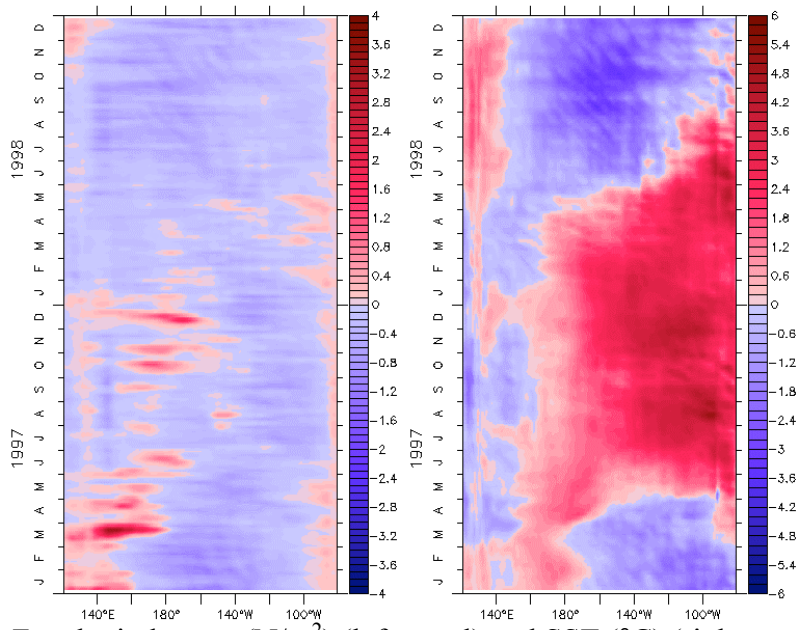

Figure A-21. Zonal wind stress (N/m^2) (left panel) and SST (°C) (right panel) anomalies of SODA_XP Group 7 from 1997 – 1998.

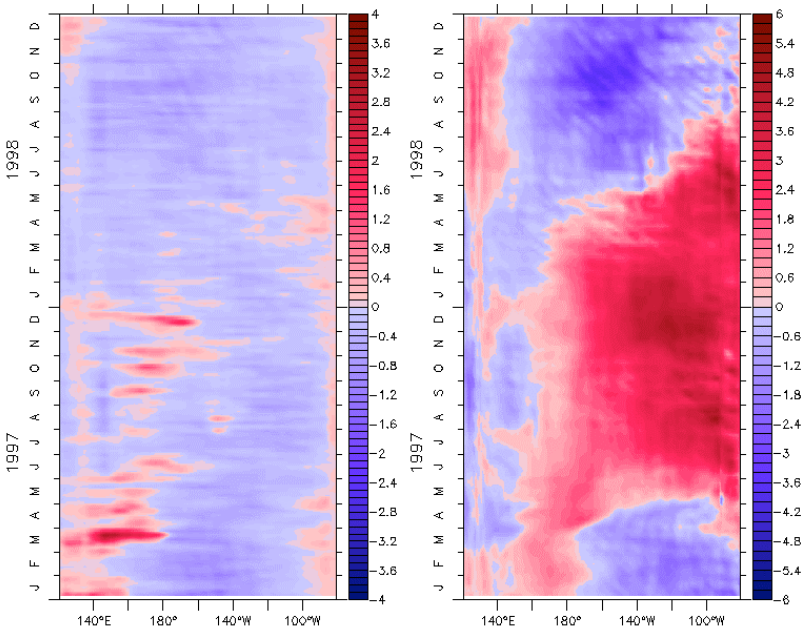

Figure A-22. Zonal wind stress (N/m^2) (left panel) and SST (°C) (right panel) anomalies of SODA_XP Group 8 from 1997 – 1998.

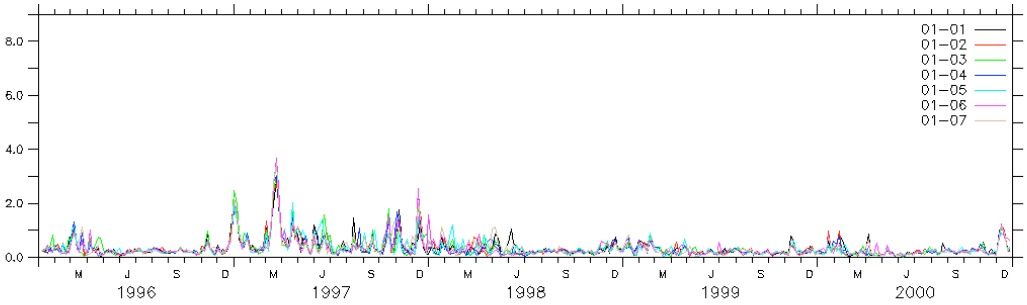

Figure A-23. Equatorial zonal wind stress maximum anomalies (N/m^2) for the 7 ensemble members of SODA_XP Group 1 from 1996-2000.

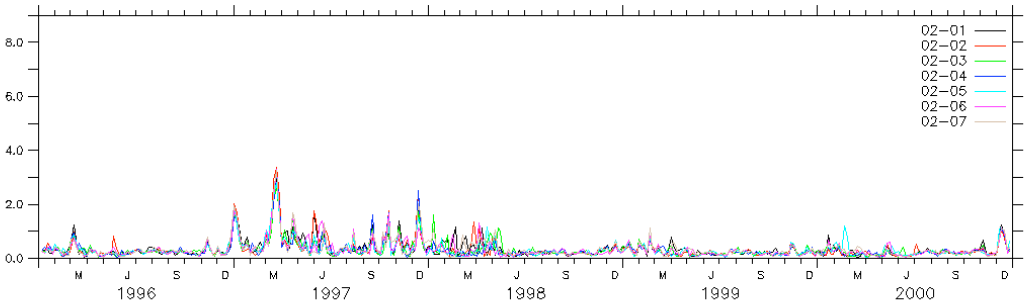

Figure A-24. Equatorial zonal wind stress maximum anomalies (N/m^2) for the 7 ensemble members of SODA_XP Group 2 from 1996-2000.

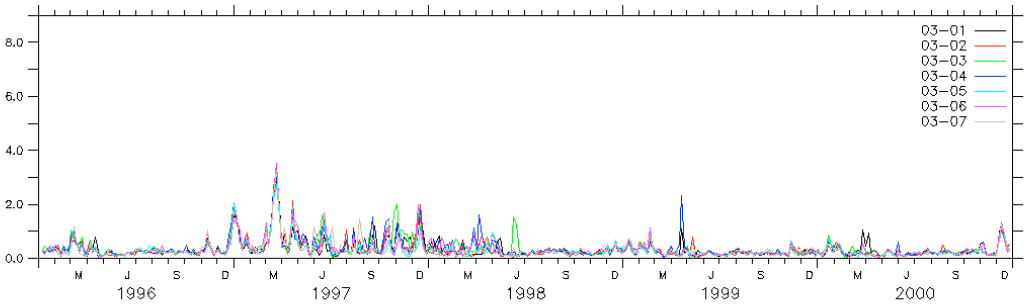

Figure A-25. Equatorial zonal wind stress maximum anomalies (N/m^2) for the 7 ensemble members of SODA_XP Group 3 from 1996-2000.

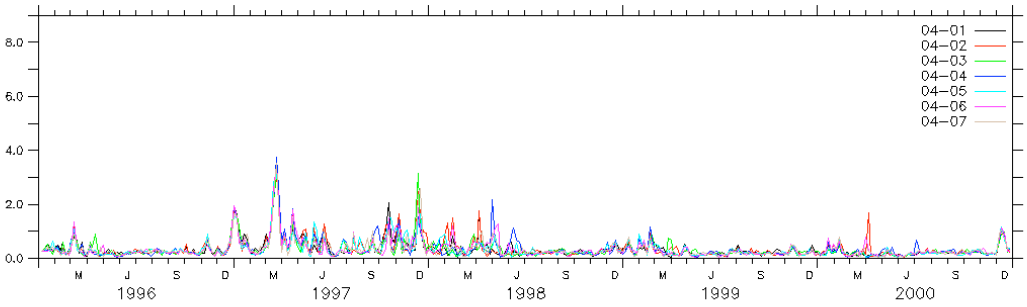

Figure A-25. Equatorial zonal wind stress maximum anomalies (N/m^2) for the 7 ensemble members of SODA_XP Group 4 from 1996-2000.

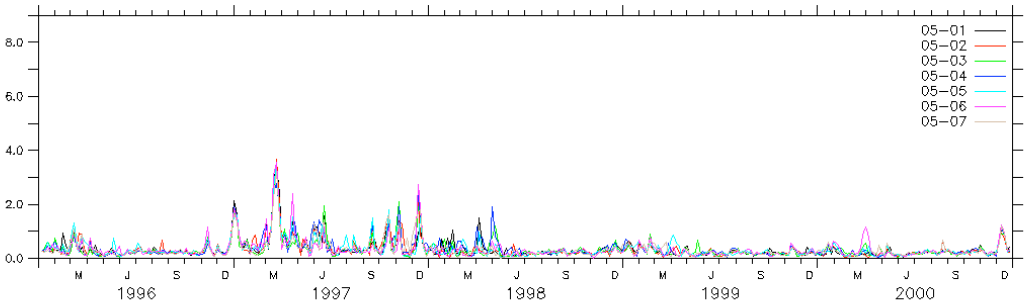

Figure A-26. Equatorial zonal wind stress maximum anomalies (N/m^2) for the 7 ensemble members of SODA_XP Group 5 from 1996-2000.

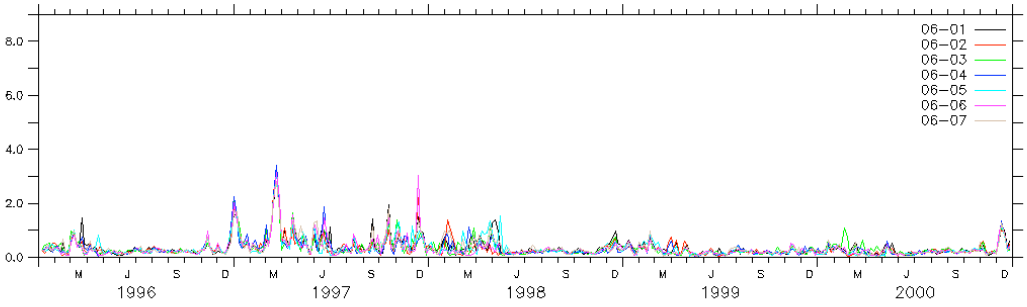

Figure A-27. Equatorial zonal wind stress maximum anomalies (N/m^2) for the 7 ensemble members of SODA_XP Group 6 from 1996-2000.

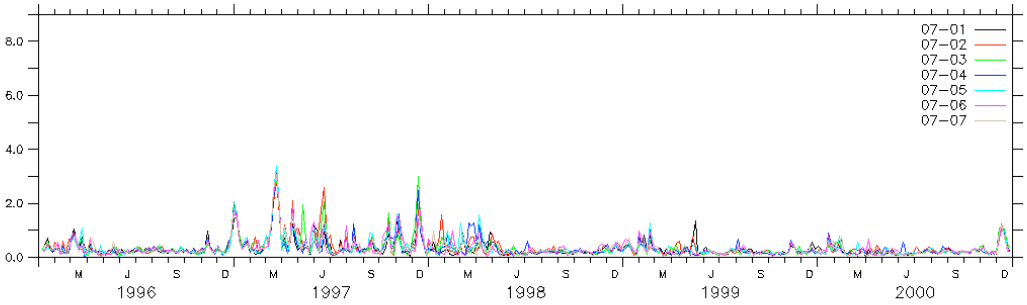

Figure A-28. Equatorial zonal wind stress maximum anomalies (N/m^2) for the 7 ensemble members of SODA_XP Group 7 from 1996-2000.

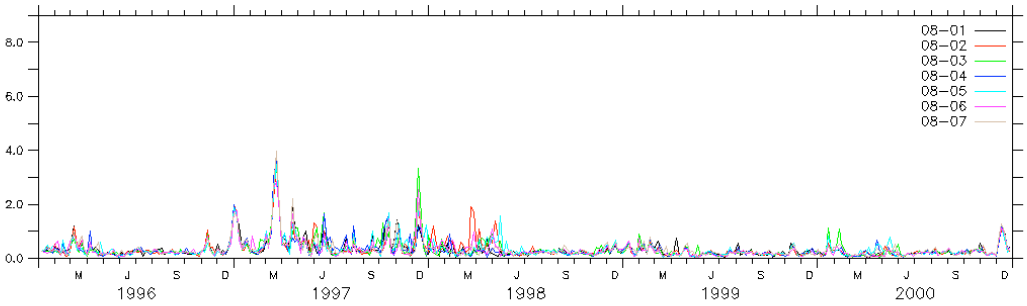

Figure A-29. Equatorial zonal wind stress maximum anomalies (N/m^2) for the 7 ensemble members of SODA_XP Group 8 from 1996-2000.